

Weighted Bayesian Cramér–Rao Bound for Mixed-Resolution Parameter Estimation

Yaniv Mazor *Student Member, IEEE* and Tirza Routtenberg, *Senior Member, IEEE*

Abstract—Mixed-resolution architectures, combining high-resolution (analog) data with coarsely quantized (e.g. 1-bit) data, are widely employed in emerging communication and radar systems to reduce hardware costs and power consumption. However, the use of coarsely quantized data introduces non-trivial trade-offs in parameter estimation tasks. In this paper, we investigate the derivation of lower bounds for such systems. In particular, we develop the weighted Bayesian Cramér–Rao bound (WBCRB) for the mixed-resolution setting with a general weight function. We demonstrate the special cases of: (i) the classical BCRB; (ii) the WBCRB that is based on the Bayesian Fisher information matrix (BFIM)–Inverse weighting; and (iii) the Aharon-Tabrikian tightest WBCRB with an optimal weight function. Based on the developed WBCRB, we propose a new method to approximate the mean-squared-error (MSE) by partitioning the estimation problem into two regions: (a) where the 1-bit quantized data is informative; and (b) where it is saturated. We apply region-specific WBCRB approximations in these regions to achieve an accurate composite MSE estimate. We derive the bounds and MSE approximation for the linear Gaussian orthonormal (LGO) model, which is commonly used in practical signal processing applications. Our simulation results demonstrate the use of the proposed bounds and approximation method in the LGO model with a scalar unknown parameter. It is shown that the WBCRB outperforms the BCRB, where the BFIM–Inverse weighting version approaches the optimal WBCRB. Moreover, it is shown that the WBCRB-based MSE approximation is tighter and accurately predicts the non-monotonic behavior of the MSE in the presence of quantization errors.

Index Terms—Mixed-resolution data; low-bit quantization; weighted Bayesian Cramér–Rao bound (WBCRB); mean-squared-error (MSE) approximation; performance analysis

I. INTRODUCTION

The estimation of unknown parameters from quantized observations arises in various applications, including wireless sensor networks (WSNs) [1]–[4], target tracking [5], and radar systems [6]. In recent years, mixed-resolution architectures, which combine high-resolution (analog) data with coarsely quantized data, such as 1-bit measurements, have been increasingly adopted in modern communication systems, radar, and massive multiple-input multiple-output (MIMO) technologies [7], [8]. These architectures offer significant benefits in terms of reduced hardware complexity, power consumption, and bandwidth requirements, making them especially attractive for systems relying on low-cost analog-to-digital converters (ADCs). For example, communication systems often require energy-efficient and cost-effective ADCs, while still demanding accurate channel estimation [9]. In such settings, parameter estimation is performed using data from multiple resolutions, posing unique challenges. While analog data remains informative across a wide range of signal-to-noise

ratios (SNRs), quantized data exhibits nonlinear behavior and becomes uninformative in high-SNR regions. This behavior results in a non-monotonic relationship between the mean-squared-error (MSE) and the SNR, with a saturation effect at high SNR where MSE performance does not improve with increasing SNR [10]–[14]; this complicates both estimator design and system analysis. Consequently, the development of performance bounds and tractable MSE expressions for estimation based on mixed analog and quantized data is crucial for reliable performance analysis and system design.

Performance bounds are fundamental tools for the analysis and design of quantized estimation systems. Several lower bounds on the non-Bayesian MSE for deterministic parameter estimation from quantized observations have been proposed, such as Cramér–Rao bounds (CRBs) for the linear Gaussian model [15]–[17], for unknown distributions [4], and for additive-controlled perturbation of the quantizer thresholds for M -level quantized observations [18]. The CRB has been developed for different applications, such as for direct position determination (DPD) [19]. The CRB for general mixed-resolution settings was discussed in [20], and for direction of arrival (DOA) estimation using a uniform linear array (ULA) in [8]. In some works, tractable approximations for the CRB in 1-bit data settings have been derived by replacing the true model with a Gaussian distribution [21] for nonlinear problems (e.g., DOA estimation). In Bayesian settings, MSE lower bounds for 1-bit quantized data with dithering have been developed in [22], [23]. The Bayesian CRB (BCRB) under quantized compressed sensing measurements has been derived in [24], and an upper bound on the BCRB for the quantized setting was proposed in [25], [26]. The CRB, hybrid CRB and BCRB for angular-domain channel estimation are all derived in [27]. MSE bounds have also been used as optimization objectives. In [18], it is shown that random dithering can significantly reduce the CRB. In [28], deterministic dithering is shown to be optimal in terms of minimizing the BCRB. The optimization of the dithering approach based on the CRB has been explored in [18]. Quantization schemes that maximize the Fisher information matrix (FIM) and minimize the CRB were developed in [29] and [30], respectively.

While these works provide valuable insights into estimation under quantization, they often lack tightness in high-SNR regimes, or fail to capture the non-monotonic behavior of the MSE of practical estimators, particularly in mixed-resolution settings. For example, in [1] it is shown that there is a significant gap between the CRB for 1-bit data and the MSE of the clairvoyant estimator. In particular, in mixed-resolution scenarios the presence of quantized data leads to complex MSE behavior that is not captured by classical bounds. In our previous work [31], we demonstrated that the classical BCRB fails to capture the non-monotonic behavior of the MSE in mixed-resolution systems, and thus, cannot be used

Yaniv Mazor and Tirza Routtenberg are with the School of Electrical and Computer Engineering Ben-Gurion University of the Negev Beer-Sheva 84105, Israel, e-mail: {mazya@post., tirzar@}bgu.ac.il. This research was supported by the ISRAEL SCIENCE FOUNDATION (Grant No. 1148/22).

as a tool for system design. This limitation underscores the need for new theoretical tools that account for both analog and quantized 1-bit measurements, provide tight bounds, and enable accurate MSE approximations across operating regimes. In this paper, we address this gap by developing the weighted Bayesian CRB (WBCRB) tailored for mixed-resolution architectures.

In this work, we consider the problem of Bayesian parameter estimation using mixed-resolution data, comprising both analog (unquantized) and 1-bit quantized measurements. First, we present the implementation of the numerical minimum mean-squared-error (MMSE) and linear minimum-mean-squared-error (LMMSE) estimators for a general threshold. Then, we derive the WBCRB tailored for mixed-resolution systems. The WBCRB is a generalization of the classical BCRB that incorporates a user-defined weight matrix to potentially yield tighter bounds. We develop three special cases of the WBCRB: 1) the classical BCRB; 2) a data-aware WBCRB based on weighting by the inverse of the FIM; and 3) the tightest WBCRB, which is obtained by computing the optimal weight function as proposed in [32]. An additional contribution here is the presentation of a novel two-regime MSE approximation method that leverages the WBCRB to accurately capture the non-monotonic behavior of the MSE across different SNR ranges. This method partitions the estimation problem into informative and saturated regions of the quantized data and applies region-specific approximations.

We demonstrate the effectiveness of the bounds and approximations for the linear Gaussian orthonormal (LGO) model, a widely used framework in signal processing applications [33]. Our simulation results show that, unlike the BCRB, which fails to reflect the MSE behavior, the proposed WBCRB variants accurately track the MSE and provide tighter alternatives. Moreover, the WBCRB-based MSE approximation closely matches the true MMSE and LMMSE performance, making it a practical and computationally efficient tool for system design in resource-constrained mixed-resolution environments.

The remainder of the paper is organized as follows: Section II presents mathematically the general mixed-resolution measurement model. Section III discusses practical estimation methods. In Section IV, we derive the general WBCRB and outline some special cases. Section V develops the new regime-aware MSE approximation method, which leverages the WBCRB. In Section VI, we apply these results to the LGO measurement model. Finally, simulation results are discussed in Section VII, and conclusions are drawn in Section VIII.

Notation: We use boldface lowercase letters to denote vectors and boldface capital letters for matrices. The identity matrix of size $M \times M$ is denoted by \mathbf{I}_M , and a vector of ones of length N is denoted by $\mathbf{1}_N$. The symbols $(\cdot)^*$, $(\cdot)^T$, and $(\cdot)^H$ represent the conjugate, transpose, and conjugate transpose operators, respectively. The notation $\mathbf{A} \succeq \mathbf{B}$ implies that $\mathbf{A} - \mathbf{B}$ is a positive semidefinite matrix. The notation $\text{diag}\{\mathbf{A}\}$ denotes the diagonal matrix containing the diagonal elements of \mathbf{A} . The m th element of the gradient vector $\nabla_{\boldsymbol{\theta}} c$ is given by $\frac{\partial c}{\partial \theta_m}$, where $\boldsymbol{\theta} = [\theta_1, \dots, \theta_M]^T$ and c is a scalar function of $\boldsymbol{\theta}$. The notations $\mathbb{E}_p[\cdot]$ and $\mathbb{E}_p[\cdot|A]$ represent the expectation and conditional expectation with respect to a given event A , respectively. All complex-valued derivatives are defined as the Wirtinger derivatives [34, ch. 1]. The distribution of a circularly symmetric complex Gaussian random vector with

mean $\boldsymbol{\mu}$ and covariance matrix $\boldsymbol{\Sigma}$ is denoted by $\mathcal{CN}(\boldsymbol{\mu}, \boldsymbol{\Sigma})$, and henceforth referred to as a complex Gaussian vector. We denote the cross-covariance matrix between \mathbf{a} and \mathbf{b} as $\mathbf{C}_{ab} = \mathbb{E}[(\mathbf{a} - \boldsymbol{\mu}_a)(\mathbf{b} - \boldsymbol{\mu}_b)^H]$, where $\mathbf{C}_a = \mathbf{C}_{aa}$, and $\boldsymbol{\mu}_a$ and $\boldsymbol{\mu}_b$ are the expectations of \mathbf{a} and \mathbf{b} , respectively. The 1-bit element-wise quantization function is applied separately on the real and imaginary parts of any $z \in \mathbb{C}$, $\text{Re}\{z\}$ and $\text{Im}\{z\}$, and is defined as

$$\mathcal{Q}(z) = \frac{1}{\sqrt{2}} \left[\begin{cases} 1, \text{Re}\{z\} \geq 0 \\ -1, \text{Re}\{z\} < 0 \end{cases} + j \begin{cases} 1, \text{Im}\{z\} \geq 0 \\ -1, \text{Im}\{z\} < 0 \end{cases} \right]. \quad (1)$$

II. MODEL AND PROBLEM FORMULATION

In this section, we present the problem of parameter estimation based on mixed-resolution data. We consider a Bayesian estimation problem where the goal is to estimate a complex-valued continuous random parameter vector, $\boldsymbol{\theta} \in \Omega_{\boldsymbol{\theta}} \in \mathbb{C}^M$, with the associated prior probability density function (PDF) $p(\boldsymbol{\theta})$, based on mixed-resolution data. The available data includes high-resolution analog measurements $\mathbf{x}_a \in \mathbb{C}^{N_a}$. This analog data can be interpreted as a model of sufficiently high-resolution measurements with negligible residual quantization noise [9]. In addition, the data includes a quantized, low-resolution measurement vector, $\mathbf{x}_q \in \mathcal{Z}^{N_q}$, which is a random vector with values in the lexicon

$$\mathcal{Z} = \left\{ \frac{1}{\sqrt{2}}(1 + j), \frac{1}{\sqrt{2}}(1 - j), \frac{1}{\sqrt{2}}(-1 + j), \frac{1}{\sqrt{2}}(-1 - j) \right\}.$$

This quantized data has been obtained using the 1-bit quantization in (1). For the sake of simplicity, we assume that \mathbf{x}_a and \mathbf{x}_q are conditionally independent given $\boldsymbol{\theta}$.

In the following, we describe the joint likelihood function in the presence of both continuous (\mathbf{x}_a and $\boldsymbol{\theta}$) and discrete (\mathbf{x}_q) random variables. The joint posterior cumulative distribution function (CDF) of \mathbf{x}_a and \mathbf{x}_q given $\boldsymbol{\theta}$ can be written as

$$\begin{aligned} F_{\mathbf{x}_a, \mathbf{x}_q | \boldsymbol{\theta}}(\boldsymbol{\alpha}, \boldsymbol{\beta} | \boldsymbol{\theta}) &= \Pr(\mathbf{x}_a \leq \boldsymbol{\alpha}, \mathbf{x}_q \leq \boldsymbol{\beta} | \boldsymbol{\theta}) \\ &= \Pr(\mathbf{x}_a \leq \boldsymbol{\alpha} | \boldsymbol{\theta}) \times \Pr(\mathbf{x}_q \leq \boldsymbol{\beta} | \boldsymbol{\theta}), \end{aligned} \quad (2)$$

where $\boldsymbol{\alpha} \in \mathbb{C}^{N_a}$ and $\boldsymbol{\beta} \in \mathcal{Z}^{N_q}$. The last equality stems from the conditional independence of \mathbf{x}_a and \mathbf{x}_q given $\boldsymbol{\theta}$.

The assumed probability space consists of the sample space $\mathbb{C}^{N_a} \times \mathcal{Z}^{N_q}$, the σ -algebra that is the product σ -algebra generated by the Borel sets on \mathbb{C}^{N_a} and the subsets of \mathcal{Z}^{N_q} , and the probability measure $\lambda^{N_a} \times \nu^{N_q}$, in which λ^{N_a} is the Lebesgue measure on \mathbb{C}^{N_a} for the continuous part, and ν^{N_q} is the counting measure on \mathcal{Z}^{N_q} for the discrete part. Let¹ $p(\mathbf{x}_a | \boldsymbol{\theta})$ be the PDF of \mathbf{x}_a with respect to (w.r.t.) λ^{N_a} , and $p(\mathbf{x}_q | \boldsymbol{\theta})$ be the PMF of \mathbf{x}_q w.r.t. ν^{N_q} . Using Bayes theorem, the conditional log-likelihood for the considered model is

$$\log p(\mathbf{x}_a | \mathbf{x}_q, \boldsymbol{\theta}) + \log p(\mathbf{x}_q | \boldsymbol{\theta}) = \log p(\mathbf{x}_a | \boldsymbol{\theta}) + \log p(\mathbf{x}_q | \boldsymbol{\theta}), \quad (3)$$

where the last equality is since, given $\boldsymbol{\theta}$, the measurement vectors \mathbf{x}_a and \mathbf{x}_q are independent. This likelihood function is derived using (2) and the Radon-Nikodym theorem [36] w.r.t. the probability measure $\lambda^{N_a} \times \nu^{N_q}$.

The goal of the considered estimation problem is to use the mixed-resolution measurements, $\mathbf{x} \triangleq [\mathbf{x}_a^T, \mathbf{x}_q^T]^T$, to estimate $\boldsymbol{\theta}$.

¹For simplicity, we denote the PDF, the probability mass function (PMF), and the mixed likelihood by $p(\cdot)$ (see p. 124 in [35])

The MMSE estimator and its associated MSE do not possess closed-form analytical expressions since the conditional PDF of θ given \mathbf{x} is intractable in the presence of quantized measurements. Numerical evaluation of the MMSE estimator is also impractical for large systems (see Section III). Similarly, the LMMSE estimator and its MSE have analytical expressions only in specific cases, such as in [7], [37]. Thus, we aim to develop closed-form performance bounds and tractable MSE approximations based on the WBCRB for performance analysis and system design in the mixed-resolution case.

Parameter estimation in mixed-resolution systems presents unique challenges due to the non-trivial behavior of the MSE. In the case of purely quantized measurements, two key regions usually emerge: (1) the low-SNR regime, where 1-bit quantized measurements convey useful information for the estimation approach; and (2) the high-SNR regime, where 1-bit quantization saturates, i.e., the measurements can be considered to always obtain a deterministic value [38]–[40]. Similarly, in mixed-resolution systems the SNR axis can be divided into three regions: 1) low SNR regime, where the 1-bit measurements are informative and the analog data is unnecessary; 2) mid-SNR regime, where both quantized and analog data contribute to the estimation process; and 3) high SNR regime (asymptotic region), occurs at the so-called “threshold point,” where the quantized data always get a single, deterministic value in the lexicon space, and thus, only analog data contributes to estimation. The non-monotonic behavior may not be captured by the BCRB [31], as is illustrated in Fig. 1 for zero quantization threshold. Identifying these regimes through new performance bounds and MSE approximations is essential for system design and performance analysis. These tools can inform resource allocation, power allocation, bit-resolution choice, and sensor selection, and serve as benchmarks for practical estimators.

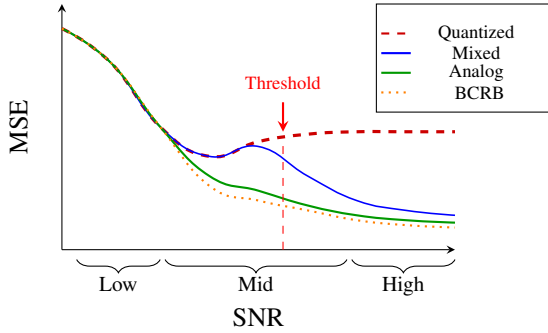


Fig. 1: Schematic graph showing MSE vs. SNR in a mixed-resolution system with a zero quantization threshold [31], showing the three regimes of low-SNR, mid-SNR, and high-SNR. The composite MSE (blue curve) exhibits non-monotonic behavior due to contributions from analog and quantized data. The analog-only MSE (green curve) decreases monotonically, while the quantized-only MSE (red dashed curve) has a distinct peak in the mid-SNR region. The BCRB (orange dotted curve) does not capture the non-monotonicity.

III. ESTIMATION METHODS

Deriving estimators and calculating their MSE under the nonlinear mixed-resolution model is analytically demanding. In this section, we present the background on two benchmark estimators: the MMSE estimator (Subsection III-A), which is

generally infeasible for large-scale problems, and the more tractable LMMSE estimator (Subsection III-B), which may have a higher MSE. Contrasting these two (approximated) estimators illustrates the intractability of MSE analysis, and highlights the need for other tools.

A. MMSE Estimator

The MMSE estimator of θ given the mixed-resolution observations \mathbf{x}_a and \mathbf{x}_q is defined as

$$\hat{\theta}_{\text{MMSE}}(\mathbf{x}_a, \mathbf{x}_q) = \mathbb{E}[\theta | \mathbf{x}_a, \mathbf{x}_q]. \quad (4)$$

Using Bayes rule and the conditional independence between \mathbf{x}_a and \mathbf{x}_q given θ , the posterior PDF of θ given the observations is

$$p(\theta | \mathbf{x}_a, \mathbf{x}_q) = \frac{p(\theta) p(\mathbf{x}_a | \theta) p(\mathbf{x}_q | \theta)}{\int_{\Omega_\theta} p(\theta) p(\mathbf{x}_a | \theta) p(\mathbf{x}_q | \theta) d\theta}. \quad (5)$$

Substituting (5) in (4), the MMSE estimator is given by

$$\hat{\theta}_{\text{MMSE}}(\mathbf{x}_a, \mathbf{x}_q) = \frac{\int_{\Omega_\theta} \theta p(\theta) p(\mathbf{x}_a | \theta) p(\mathbf{x}_q | \theta) d\theta}{\int_{\Omega_\theta} p(\theta) p(\mathbf{x}_a | \theta) p(\mathbf{x}_q | \theta) d\theta}. \quad (6)$$

In general, the integrals on the r.h.s. of (6) lack closed-form solutions due to the discrete nature of \mathbf{x}_q and the nonlinearities in its conditional PMF.

Direct numerical evaluation of the integrals in (6) faces the curse of dimensionality, as the number of grid points, M , grows exponentially with the dimension of θ , which is impractical for high-dimensional problems (see, e.g., [41]). An alternative is to approximate the MMSE estimator using Monte Carlo methods [42], [43, Ch. 3], which avoids discretization and scales better with M . Specifically, (6) can be rewritten as

$$\hat{\theta}_{\text{MMSE}}(\mathbf{x}_a, \mathbf{x}_q) = \frac{\mathbb{E}_\theta[\theta p(\mathbf{x}_a | \theta) p(\mathbf{x}_q | \theta)]}{\mathbb{E}_\theta[p(\mathbf{x}_a | \theta) p(\mathbf{x}_q | \theta)]}. \quad (7)$$

It should be noted that the expectations in (7) are taken over the prior $p(\theta)$ (and not w.r.t. the posterior PDF), treating \mathbf{x}_a and \mathbf{x}_q as deterministic vectors. To emphasize this distinction, we use the notation $\mathbb{E}_\theta[\cdot]$.

By the Strong Law of Large Numbers, the sample mean converges almost surely to the true expectation. Hence, given S independent and identically distributed (i.i.d.) samples $\{\theta^{(s)}\}_{s=1}^S$ drawn from the prior PDF $p(\theta)$, the MMSE estimator in (7) can be approximated as

$$\hat{\theta}_{\text{MMSE}}(\mathbf{x}_a, \mathbf{x}_q) \approx \frac{\sum_{s=1}^S \theta^{(s)} p(\mathbf{x}_a | \theta^{(s)}) p(\mathbf{x}_q | \theta^{(s)})}{\sum_{s=1}^S p(\mathbf{x}_a | \theta^{(s)}) p(\mathbf{x}_q | \theta^{(s)})}. \quad (8)$$

Unlike grid-based numerical integration, the variances of the empirical estimators in (8) are independent of the dimension M of θ [42], [43], making it better-suited for high-dimensional data. However, a large number of samples S is still required for accuracy, especially when $p(\mathbf{x}_a | \theta)$ and $p(\mathbf{x}_q | \theta)$ are sharply concentrated. Advanced techniques, such as importance sampling [44] or Markov Chain Monte Carlo (MCMC), can be employed to reduce the MSE and accelerate convergence. The overall procedure is summarized in Algorithm 1.

Using the law of total expectation, the MSE matrix of the MMSE estimator can be written as

$$\begin{aligned} & \text{MSE}(\hat{\theta}(\mathbf{x}_a, \mathbf{x}_q)) \\ &= \mathbb{E} \left[\mathbb{E} \left[(\hat{\theta}(\mathbf{x}_a, \mathbf{x}_q) - \theta)(\hat{\theta}(\mathbf{x}_a, \mathbf{x}_q) - \theta)^H | \mathbf{x}_a, \mathbf{x}_q \right] \right], \end{aligned} \quad (9)$$

Algorithm 1: Monte Carlo MMSE Estimator

Input:

- Distributions: $p(\theta)$, $p(\mathbf{x}_a|\theta)$, $p(\mathbf{x}_q|\theta)$
- Number of samples S
- Single-test measurements: \mathbf{x}_a , \mathbf{x}_q

Output: Approximate MMSE estimator $\hat{\theta}(\mathbf{x}_a, \mathbf{x}_q)$.

- 1: **for** $s = 1, \dots, S$ **do**
- 2: Draw the sample $\theta^{(s)} \sim p(\theta)$
- 3: Compute the weights $w^{(s)} = p(\mathbf{x}_a|\theta^{(s)})p(\mathbf{x}_q|\theta^{(s)})$
- 4: **end for**
- 5: Approximate the MMSE in (7) as

$$\hat{\theta}(\mathbf{x}_a, \mathbf{x}_q) = \frac{\sum_{s=1}^S \theta^{(s)} w^{(s)}}{\sum_{s=1}^S w^{(s)}}.$$

for $\hat{\theta}(\mathbf{x}_a, \mathbf{x}_q) = \hat{\theta}_{\text{MMSE}}(\mathbf{x}_a, \mathbf{x}_q)$. Numerically evaluating the MSE matrix in (9) is significantly more demanding than computing the MMSE estimator itself, as it requires an additional expectation over all possible values of \mathbf{x}_a and \mathbf{x}_q . Specifically, the inner expectation in (9) involves computing the posterior covariance matrix, which is highly nonlinear in the presence of discrete variables and non-Gaussian distributions. The outer expectation requires integration over the continuous variable \mathbf{x}_a and summation over all discrete lexicon values of \mathbf{x}_q , where the computational complexity increases as N_a and N_q increase. These challenges render the direct computation of the Bayesian MSE matrix impractical in high-dimensional settings, even when employing the Monte Carlo-based approximation that is summarized in Algorithm 2. This empirical MSE is obtained as the sample mean of the squared error across K trials. The accuracy of this method depends on K being sufficiently large to ensure convergence.

Algorithm 2: Monte Carlo MSE Matrix

Input:

- Distributions: $p(\theta)$, $p(\mathbf{x}_a|\theta)$, $p(\mathbf{x}_q|\theta)$
- Number of trials K for MSE evaluation
- Number of samples S

Output: Empirical MSE of the MMSE estimator

- 1: Initialize $\mathbf{e}_{\text{total}} = \mathbf{0}$
 - 2: **for** $k = 1, \dots, K$ **do**
 - 3: Draw the sample $\theta_0^{(k)} \sim p(\theta)$
 - 4: Generate measurements $\mathbf{x}_a^{(k)}$ and $\mathbf{x}_q^{(k)}$ from $p(\mathbf{x}_a|\theta_0^{(k)})$ and $p(\mathbf{x}_q|\theta_0^{(k)})$, respectively
 - 5: Compute the approximated MMSE estimator $\hat{\theta}^{(k)} = \hat{\theta}(\mathbf{x}_a^{(k)}, \mathbf{x}_q^{(k)})$ using S samples via Algorithm 1
 - 6: Update the squared error $\mathbf{e}_{\text{total}} \leftarrow \mathbf{e}_{\text{total}} + (\hat{\theta}^{(k)} - \theta_0^{(k)})(\hat{\theta}^{(k)} - \theta_0^{(k)})^H$
 - 7: **end for**
 - 8: Compute the empirical Bayesian MSE as $\frac{1}{K} \mathbf{e}_{\text{total}}$.
-

B. LMMSE Estimator

The LMMSE estimator is widely used in scenarios involving quantized data [11], [45], [46]. While it is generally suboptimal compared to the MMSE estimator, it often has closed-form expressions or enables tractable numerical approximations, and its computational efficiency makes it well-suited for real-time applications with limited resources [45].

The analytical LMMSE estimator of θ is

$$\hat{\theta}_{\text{LMMSE}}(\mathbf{x}_a, \mathbf{x}_q) = \mathbb{E}[\theta] + \mathbf{C}_{\theta\mathbf{x}} \mathbf{C}_{\mathbf{x}}^{-1} (\mathbf{x} - \mathbb{E}[\mathbf{x}]), \quad (10)$$

and its MSE is given by

$$\text{MSE}(\hat{\theta}_{\text{LMMSE}}(\mathbf{x}_a, \mathbf{x}_q)) = \Sigma_{\theta} - \mathbf{C}_{\theta\mathbf{x}} \mathbf{C}_{\mathbf{x}}^{-1} \mathbf{C}_{\theta\mathbf{x}}^H. \quad (11)$$

For the mixed-resolution case, $\mathbb{E}[\mathbf{x}] = \mathbb{E}[\mathbf{x}_a^T, \mathbf{x}_q^T]^T$ and

$$\mathbf{C}_{\mathbf{x}} = \begin{bmatrix} \mathbf{C}_{\mathbf{x}_a} & \mathbf{C}_{\mathbf{x}_a\mathbf{x}_q} \\ \mathbf{C}_{\mathbf{x}_q\mathbf{x}_a} & \mathbf{C}_{\mathbf{x}_q} \end{bmatrix}, \quad \mathbf{C}_{\theta\mathbf{x}} = [\mathbf{C}_{\theta\mathbf{x}_a} \quad \mathbf{C}_{\theta\mathbf{x}_q}]. \quad (12)$$

In most practical cases, the expectations and covariance matrices in (10)–(11) do not admit closed-form expressions, and are replaced by sample mean and sample covariance matrices (SCM) estimates based on a dataset of i.i.d. samples, $\mathcal{D} = \{\theta^{(k)}, \mathbf{x}_a^{(k)}, \mathbf{x}_q^{(k)}\}_{k=1}^K$. For example, $\mathbf{C}_{\mathbf{x}_q}$ is replaced with

$$\hat{\mathbf{C}}_{\mathbf{x}_q} = \frac{1}{K} \sum_{k=1}^K (\mathbf{x}_q^{(k)} - \bar{\mathbf{x}}_q)(\mathbf{x}_q^{(k)} - \bar{\mathbf{x}}_q)^H, \quad (13)$$

where $\bar{\mathbf{x}}_q = \frac{1}{K} \sum_{k=1}^K \mathbf{x}_q^{(k)}$. Replacing the expectations and covariances with empirical estimates yields the numerical LMMSE estimator, which minimizes the empirical MSE [47] $\frac{1}{K} \sum_{k=1}^K \|\theta^{(k)} - \hat{\theta}\|_2^2$. As $K \rightarrow \infty$, the SCMs converge to the true covariance matrices ([48], p. 728 in [49]), ensuring asymptotic consistency of this estimator [48], [49].

When partial statistical knowledge is available, e.g., under the LGO model, one may employ the partially numeric LMMSE estimator [31], which uses known covariance matrices for the analog part and estimates only the covariances involving quantized data. It converges to the LMMSE estimator as K increases and often outperforms the fully numerical approach. Finally, the MSE of the LMMSE estimator can be computed in two ways: (i) empirically, as in Algorithm 2 by replacing the estimator in Step 4 with (10), or (ii) directly via (11). Both approaches require SCM computation, which becomes expensive as N_a and N_q grow. Moreover, since the LMMSE estimator is suboptimal, its MSE serves only as an upper bound and may not reflect true system performance.

IV. WBCRB FOR MIXED-RESOLUTION DATA

In this section, we develop the WBCRB for mixed-resolution observations, which incorporates a flexible weight matrix, enabling tighter and more informative bounds across varying SNR regimes. In Subsection IV-A, we discuss the associated regularity conditions. In Subsection IV-B, we present the general bound, and in Subsection IV-C, special cases are discussed. We use the general model from Section II and a Hermitian, positive-definite weight matrix $\mathbf{W}(\theta) \in \mathbb{C}^{M \times M}$, whose entries are differentiable functions, i.e., it has well-defined componentwise Wirtinger derivatives.

A. Regularity Conditions

In this subsection, we establish the regularity conditions required for the derivation of the WBCRB in the mixed-resolution setting. Classical formulations of the BCRB and WBCRB assume continuous observation vectors (see, e.g., [32], [50]), whereas for purely discrete observation vectors, suitable regularity conditions of the BCRB are presented in [22]. The following WBCRB regularity conditions generalize these assumptions to the mixed-resolution model defined in Section II, where the observation vector \mathbf{x} comprises both

continuous and discrete components, \mathbf{x}_a and \mathbf{x}_q , and the log-likelihood function in (3). The conditions are as follows:

- 1) **Differentiability:** The joint log-likelihood function in (3) is differentiable w.r.t. $\boldsymbol{\theta}$, and the associated Bayesian Fisher information matrix (BFIM), \mathbf{J} , is a well-defined and non-singular matrix.
- 2) **Integrability:** The score function $\nabla_{\boldsymbol{\theta}} \log p(\boldsymbol{\theta}) p(\mathbf{x}_a|\boldsymbol{\theta}) p(\mathbf{x}_q|\boldsymbol{\theta})$ and its derivatives w.r.t. $\boldsymbol{\theta}$ are absolutely integrable w.r.t. the continuous variables $\boldsymbol{\theta}$ and \mathbf{x}_a , and summable w.r.t. the discrete variable \mathbf{x}_q .
- 3) **Boundary Conditions:** For each $m \in \{1, \dots, M\}$, and for every $\mathbf{x}_a \in \mathbb{C}^{N_a}$ and $\mathbf{x}_q \in \mathbb{Z}^{N_q}$, the conditional PDF and PMF decay fast enough as $|\theta_m| \rightarrow \infty$ such that integration-by-parts introduces no residual boundary terms in all relevant integrations. In particular, we assume that for all indices $l, n, k, m \in \{1, \dots, M\}$ and all $\mathbf{x}_a \in \mathbb{C}^{N_a}$, $\mathbf{x}_q \in \mathbb{C}^{N_q}$ and for the Hermitian matrix $\mathbf{W}(\boldsymbol{\theta}) \in \mathbb{C}^{M \times M}$, the following limits hold:

$$\lim_{|\theta_m| \rightarrow \infty} \theta_m [\mathbf{W}(\boldsymbol{\theta})]_{k,m}^* p(\boldsymbol{\theta}) p(\mathbf{x}_a|\boldsymbol{\theta}) p(\mathbf{x}_q|\boldsymbol{\theta}) = 0, \quad (14a)$$

$$\lim_{|\theta_m| \rightarrow \infty} [\mathbf{W}(\boldsymbol{\theta})]_{k,m}^* \frac{\partial [\mathbf{W}(\boldsymbol{\theta})]_{n,l}}{\partial \theta_l^*} p(\boldsymbol{\theta}) = 0. \quad (14b)$$

- 4) **Smoothness:** The conditional expectations of the score functions for the analog and quantized data vanish:

$$\mathbb{E}_{\mathbf{x}_a|\boldsymbol{\theta}} [\nabla_{\boldsymbol{\theta}} \log p(\mathbf{x}_a|\boldsymbol{\theta})|\boldsymbol{\theta}] = \mathbf{0}, \quad (15a)$$

$$\mathbb{E}_{\mathbf{x}_q|\boldsymbol{\theta}} [\nabla_{\boldsymbol{\theta}} \log p(\mathbf{x}_q|\boldsymbol{\theta})|\boldsymbol{\theta}] = \mathbf{0}. \quad (15b)$$

Discussion: The extension of the WBCRB to mixed-resolution observations requires paying attention to the co-existence of continuous and discrete variables. In particular, integrals are replaced with finite summations for the discrete variables \mathbf{x}_q , as presented e.g., in Condition 2. Conditions 1-4 are consistent with those previously established for fully discrete [22] and continuous models [32]. Condition 2 allows us to exchange differentiation and expectation via the dominated-convergence theorem. Formally, $\nabla_{\boldsymbol{\theta}} \mathbb{E}[h(\boldsymbol{\theta}, \mathbf{x})] = \mathbb{E}[\nabla_{\boldsymbol{\theta}} h(\boldsymbol{\theta}, \mathbf{x})]$, for any measurable function $h(\boldsymbol{\theta}, \mathbf{x})$, where the outer expectation (w.r.t. \mathbf{x}_q) is a finite sum in this case.

For the BCRB (obtained for $\mathbf{W}(\boldsymbol{\theta}) = \mathbf{I}$) and continuous observation only, Conditions (14a)–(14b) reduce to the familiar requirement that the joint PDF vanishes at the edges, $\lim_{\theta_m \rightarrow \pm\infty} \theta_m p(\boldsymbol{\theta}, \mathbf{x}_a) = 0$ (see, e.g., [51, Eq. (4.178)]). In the weighted case, an extra decay condition, (14b), is necessary because the integration-by-parts step multiplies the PDF and PMF by $\mathbf{W}(\boldsymbol{\theta})$ and its derivatives. For Condition 4, the continuous part in (15a) is automatic when the PDF is differentiable and integrable, if the support of $p(\mathbf{x}_a|\boldsymbol{\theta})$ is independent of $\boldsymbol{\theta}$ [51]. For the mixed-resolution case, (15b) must be stated explicitly to guarantee that the BFIM decomposes to analog, quantized, and prior contributions, as presented in the following.

B. General WBCRB

We now present the main theorem of the WBCRB. To this end, we first develop the BFIM term. Under Conditions 1 and 2 from Section IV-A, the BFIM for our model is well-defined. We use the fact that the BFIM satisfies [34, p. 173]

$$\mathbf{J} = \mathbf{J}_{\boldsymbol{\theta}} + \mathbb{E}_{\boldsymbol{\theta}}[\mathbf{J}_{\mathbf{x}|\boldsymbol{\theta}}(\boldsymbol{\theta})], \quad (16)$$

where the prior FIM is defined as

$$\mathbf{J}_{\boldsymbol{\theta}} \triangleq \mathbb{E}_{\boldsymbol{\theta}}[\nabla_{\boldsymbol{\theta}}^H \log p(\boldsymbol{\theta}) \nabla_{\boldsymbol{\theta}} \log p(\boldsymbol{\theta})] \quad (17)$$

and $\mathbf{J}_{\mathbf{x}|\boldsymbol{\theta}}(\boldsymbol{\theta})$ is the posterior FIM. In addition, using (3) and (15), the posterior FIM is given by

$$\mathbb{E}_{\boldsymbol{\theta}}[\mathbf{J}_{\mathbf{x}|\boldsymbol{\theta}}(\boldsymbol{\theta})] = \mathbb{E}_{\boldsymbol{\theta}}[\mathbf{J}_{\mathbf{x}_a|\boldsymbol{\theta}}(\boldsymbol{\theta})] + \mathbb{E}_{\boldsymbol{\theta}}[\mathbf{J}_{\mathbf{x}_q|\boldsymbol{\theta}}(\boldsymbol{\theta})], \quad (18)$$

where the FIMs based on each set of measurements \mathbf{x}_a and \mathbf{x}_q , respectively, given $\boldsymbol{\theta}$, are (see, e.g., [22], [52])

$$\mathbf{J}_{\mathbf{x}_a|\boldsymbol{\theta}}(\boldsymbol{\theta}) \triangleq \mathbb{E}_{\mathbf{x}_a|\boldsymbol{\theta}} [\nabla_{\boldsymbol{\theta}}^H \log p(\mathbf{x}_a|\boldsymbol{\theta}) \nabla_{\boldsymbol{\theta}} \log p(\mathbf{x}_a|\boldsymbol{\theta})|\boldsymbol{\theta}], \quad (19a)$$

$$\mathbf{J}_{\mathbf{x}_q|\boldsymbol{\theta}}(\boldsymbol{\theta}) \triangleq \mathbb{E}_{\mathbf{x}_q|\boldsymbol{\theta}} [\nabla_{\boldsymbol{\theta}}^H \log p(\mathbf{x}_q|\boldsymbol{\theta}) \nabla_{\boldsymbol{\theta}} \log p(\mathbf{x}_q|\boldsymbol{\theta})|\boldsymbol{\theta}]. \quad (19b)$$

By substituting these definitions in (16), we obtain the following structure of the BFIM for this case:

$$\mathbf{J} = \mathbf{J}_{\boldsymbol{\theta}} + \mathbb{E}_{\boldsymbol{\theta}}[\mathbf{J}_{\mathbf{x}_a|\boldsymbol{\theta}}(\boldsymbol{\theta})] + \mathbb{E}_{\boldsymbol{\theta}}[\mathbf{J}_{\mathbf{x}_q|\boldsymbol{\theta}}(\boldsymbol{\theta})]. \quad (20)$$

In addition, we define the following terms:

$$v_k(\boldsymbol{\theta}) \triangleq \sum_{m=1}^M \frac{\partial [\mathbf{W}(\boldsymbol{\theta})]_{k,m}}{\partial \theta_m^*}, \quad k = 1, \dots, M, \quad (21)$$

$$[\mathbf{A}]_{n,k} \triangleq -\mathbb{E} \left[\sum_{m=1}^M \frac{\partial ([\mathbf{W}(\boldsymbol{\theta})]_{n,m} v_k^*(\boldsymbol{\theta}))}{\partial \theta_m^*} \right], \quad (22)$$

$k, n = 1, \dots, M$, and

$$\begin{aligned} \mathbf{G} = & \mathbb{E}[\mathbf{W}(\boldsymbol{\theta}) \nabla_{\boldsymbol{\theta}}^H \log p(\boldsymbol{\theta}) p(\mathbf{x}_a|\boldsymbol{\theta}) p(\mathbf{x}_q|\boldsymbol{\theta}) \\ & \times \nabla_{\boldsymbol{\theta}} \log p(\boldsymbol{\theta}) p(\mathbf{x}_a|\boldsymbol{\theta}) p(\mathbf{x}_q|\boldsymbol{\theta}) \mathbf{W}^H(\boldsymbol{\theta})] \\ & + \mathbf{A} + \mathbf{A}^H + \mathbb{E}[\mathbf{v}(\boldsymbol{\theta}) \mathbf{v}^H(\boldsymbol{\theta})]. \end{aligned} \quad (23)$$

It can be seen that the matrix \mathbf{G} is a positive-definite matrix, where, except for the first term and the computation of the expectations, all of its components depend only on the chosen weight matrix $\mathbf{W}(\boldsymbol{\theta})$ and its derivatives.

Theorem 1 (Mixed-resolution WBCRB): Assume the model stated in Section II with $\boldsymbol{\theta} \in \Omega_{\boldsymbol{\theta}} \subset \mathbb{C}^M$, $\mathbf{x}_a \in \mathbb{C}^{N_a}$, and $\mathbf{x}_q \in \mathbb{Z}^{N_q}$, and where \mathbf{x}_a and \mathbf{x}_q are conditionally independent given $\boldsymbol{\theta}$. In addition, suppose that Conditions 1-4 hold. Then, the MSE matrix of any estimator $\hat{\boldsymbol{\theta}}(\mathbf{x}_a, \mathbf{x}_q)$ satisfies

$$\mathbb{E}[(\hat{\boldsymbol{\theta}}(\mathbf{x}_a, \mathbf{x}_q) - \boldsymbol{\theta})(\hat{\boldsymbol{\theta}}(\mathbf{x}_a, \mathbf{x}_q) - \boldsymbol{\theta})^H] \succeq \text{WBCRB}, \quad (24)$$

where

$$\text{WBCRB} \triangleq \mathbb{E}[\mathbf{W}(\boldsymbol{\theta})] \mathbf{G}^{-1} \mathbb{E}[\mathbf{W}^H(\boldsymbol{\theta})], \quad (25)$$

in which \mathbf{G} is defined in (23).

Proof: The proof appears in Appendix A. ■

In the supplemental material attached to this paper, we discuss the extension of this theorem to a widely-linear lower bound on the MSE of the augmented complex-valued error vector.

C. Special Cases

We next examine several choices of the weighting matrix $\mathbf{W}(\boldsymbol{\theta})$, each yielding a particular bound of the general WBCRB form of Theorem 1.

1) *BCRB*: By choosing $\mathbf{W}(\boldsymbol{\theta}) = \mathbf{I}$, it can be seen from (21) and (22) that we get $\mathbf{v}(\boldsymbol{\theta}) = \mathbf{0}$ and $\mathbf{A} = \mathbf{0}$. Thus, (23) implies that in this case

$$\mathbf{G} = \mathbb{E}[\nabla_{\boldsymbol{\theta}}^H \log p(\boldsymbol{\theta}) p(\mathbf{x}_a|\boldsymbol{\theta}) p(\mathbf{x}_q|\boldsymbol{\theta}) \times \nabla_{\boldsymbol{\theta}} \log p(\boldsymbol{\theta}) p(\mathbf{x}_a|\boldsymbol{\theta}) p(\mathbf{x}_q|\boldsymbol{\theta})] = \mathbf{J}, \quad (26)$$

where \mathbf{J} is the BFIM defined in (20). Thus, the WBCRB from (25) in this case is reduced to

$$\text{WBCRB} = \mathbf{J}^{-1} = \text{BCRB}, \quad (27)$$

which is the classical BCRB. The BCRB under the LGO model is discussed in [31] and in Section VI.

2) *FIM-Inverse Weighting*: A common data-aware weighting choice is the inverse of the internal term of the BFIM before computing the expectation w.r.t. $\boldsymbol{\theta}$. That is, to take

$$\mathbf{W}(\boldsymbol{\theta}) = \tilde{\mathbf{J}}^{-1}(\boldsymbol{\theta}), \quad (28)$$

where

$$\tilde{\mathbf{J}}(\boldsymbol{\theta}) \triangleq \nabla_{\boldsymbol{\theta}}^H \log p(\boldsymbol{\theta}) \nabla_{\boldsymbol{\theta}} \log p(\boldsymbol{\theta}) + \mathbf{J}_{\mathbf{x}_a|\boldsymbol{\theta}}(\boldsymbol{\theta}) + \mathbf{J}_{\mathbf{x}_q|\boldsymbol{\theta}}(\boldsymbol{\theta}). \quad (29)$$

It can be seen that $\mathbb{E}_{\boldsymbol{\theta}}[\mathbf{W}^{-1}(\boldsymbol{\theta})] = \mathbb{E}_{\boldsymbol{\theta}}[\tilde{\mathbf{J}}(\boldsymbol{\theta})] = \mathbf{J}$, where \mathbf{J} is defined in (16). By substituting (28) into (23), we get

$$\mathbf{G} = \mathbb{E}[\mathbf{W}(\boldsymbol{\theta})] + \mathbf{A} + \mathbf{A}^H + \mathbb{E}[\mathbf{v}(\boldsymbol{\theta})\mathbf{v}^H(\boldsymbol{\theta})], \quad (30)$$

that together with (28) defined the WBCRB in (25) for this choice of weighting matrix $\mathbf{W}(\boldsymbol{\theta})$. In the simulations, we demonstrate that this choice offers both analytical tractability and competitive performance across the tested scenarios.

The equality in (24) holds (i.e., the bound is tight) iff $\mathbf{J}_{\mathbf{x}|\boldsymbol{\theta}}$ defined in (19) is independent of $\boldsymbol{\theta}$ [32]. For example, in the pure analog Gaussian case in a linear additive model, this condition is satisfied, and choosing $\mathbf{W}(\boldsymbol{\theta}) = \mathbf{J}_{\mathbf{x}_q|\boldsymbol{\theta}}^{-1}$ yields a tight bound (also, in this case the WBCRB coincides with the conventional BCRB as well).

For the matrix \mathbf{G} , the first term in (30) reflects the chosen weight matrix $\mathbf{W}(\boldsymbol{\theta})$, while the remaining three terms depend on the derivatives of the weight matrix. If these derivatives (i.e., $|v_k(\boldsymbol{\theta})|$, $k = 1, \dots, M$) are significantly smaller than the elements of $\mathbf{W}(\boldsymbol{\theta})$ from (28), then these three terms are negligible and (30) is reduced to $\mathbf{G} \approx \mathbb{E}[\mathbf{W}(\boldsymbol{\theta})]$. In addition, in the asymptotic case of large N_a, N_q , the prior information is neglected. In this case, the bound defined by (25), (28), and (30) can be computed using expectation w.r.t. the prior as

$$\text{WBCRB} \approx \mathbb{E}_{\boldsymbol{\theta}}[(\mathbf{J}_{\mathbf{x}_a|\boldsymbol{\theta}}(\boldsymbol{\theta}) + \mathbf{J}_{\mathbf{x}_q|\boldsymbol{\theta}}(\boldsymbol{\theta}))^{-1}] = \text{ECRB}. \quad (31)$$

The r.h.s. of (31) is the expected CRB [51, eq. 39] for mixed-resolution data. Using Jensen's inequality, (31) implies that for a high number of measurements $N_a + N_q$, we get

$$\text{ECRB} \succeq \text{BCRB}. \quad (32)$$

Thus, under (31), the WBCRB appears to yield a tighter bound than the BCRB as long as BFIM is non-singular.

The term in (31) is valid for an asymptotic number of observations, but not for an asymptotic SNR. In particular, for pure 1-bit systems, the data BFIM $\mathbf{J}_{\mathbf{x}_q|\boldsymbol{\theta}}(\boldsymbol{\theta})$ is a highly nonlinear function of $\boldsymbol{\theta}$, and the derivative terms in \mathbf{G} generally do not vanish for a finite number of measurements. In contrast, in pure analog systems or in mixed-resolution systems where the analog observations dominate as the SNR increases, the chosen

weight matrix from (28) is typically smooth and well-behaved, leading to vanishing derivative terms and a valid reduction of the WBCRB to the expected CRB as in (31). In general, even in the non-asymptotic case, the WBCRB with $\mathbf{W}(\boldsymbol{\theta})$ from (28) offers a tighter and more reliable performance bound than the BCRB, as shown in the simulations.

3) *Optimal WBCRB*: For the sake of simplicity, we present the optimal WBCRB for the scalar case ($M = 1$), as derived in [32]. We consider a finite parameter space $\Omega_{\boldsymbol{\theta}}$ and some test points, $\theta_1, \dots, \theta_L$, which are obtained from sampled parameters over $\Omega_{\boldsymbol{\theta}}$ with Δ spacing. Then, we select the weighting vector (instead of the matrix $\mathbf{W}(\boldsymbol{\theta})$, since we are estimating a scalar), as

$$\mathbf{w}(\boldsymbol{\theta}) = \frac{(\mathbf{Z}\mathbf{F} + \bar{\Psi})^{-1} \mathbf{f}}{\mathbf{f}^T (\mathbf{Z}\mathbf{F} + \bar{\Psi})^{-1} \mathbf{f}}, \quad (33)$$

where $\mathbf{f} = \Delta \cdot [p_{\theta}(\theta_1), \dots, p_{\theta}(\theta_L)]^T$, $\mathbf{F} = \text{diag}(\mathbf{f})$, $\mathbf{Z} = \text{diag}(\tilde{J}(\theta_1), \dots, \tilde{J}(\theta_L))$, in which $\tilde{J}(\theta)$ is defined in (29). In addition, \mathbf{K} is a discrete-derivative matrix:

$$\mathbf{K}_{nm} = \frac{1}{\Delta} \begin{cases} 1 & n = m \\ -1 & n = m + 1 \\ 0 & \text{otherwise} \end{cases}, \quad (34)$$

and $\bar{\Psi} = -(\mathbf{F}\mathbf{K}\mathbf{K} + (\mathbf{F}\mathbf{K}\mathbf{K})^T + \mathbf{K}^T \mathbf{F}\mathbf{K})$. Substituting (33) in (25), results in the tightest WBCRB [32]:

$$\text{WBCRB} = \mathbf{f}^T (\mathbf{Z}\mathbf{F} + \bar{\Psi})^{-1} \mathbf{f}. \quad (35)$$

V. MSE APPROXIMATION METHOD

In nonlinear Bayesian estimation with quantized measurements, classical lower bounds, such as the BCRB, often fail to capture the non-monotonic behavior of the MSE across the SNR range, as illustrated in Fig. 1 and discussed in [31]. This issue is especially pronounced in mixed-resolution systems. At low and moderate SNR levels, quantized observations provide useful information; however, at high SNR levels, the quantized outputs saturate, i.e., converge to constant values (e.g., all-ones), and convey only coarse region or sign-level details [53]–[55]. To address this, we propose a practical MSE approximation method that leverages the WBCRB derived in Section IV, while avoiding computationally intensive Monte Carlo simulations of the estimator. The method exploits the regime-switching behavior of quantized data by combining the WBCRB (in the informative regime) with an analog-only MSE approximation (in the saturation regime). This approach is reminiscent of the method of interval estimation (MIE), which approximates performance under threshold effects by partitioning the parameter space into informative and non-informative regions [56, ch. 4.4.2], [57].

The non-monotonic behavior arises because, as the SNR increases, the noise becomes negligible and the quantized output \mathbf{x}_q converges to a deterministic function of $\boldsymbol{\theta}$. In this regime, repeated observations yield identical quantized values, and the posterior distribution is effectively determined solely by the prior and any analog measurements, with negligible impact of \mathbf{x}_q . Formally, this property can be written as

$$p(\mathbf{x}_q|\boldsymbol{\theta}) \xrightarrow{\text{SNR} \rightarrow \infty} \begin{cases} 1 & \mathbf{x}_q = \mathbf{c}(\boldsymbol{\theta}) \\ 0 & \text{otherwise} \end{cases}, \quad (36)$$

where $\mathbf{c}(\boldsymbol{\theta})$ is a deterministic mapping from the parameter space to the quantized alphabet, independent of the noise realization [14], [13, p. 112]. We define the *decision cell* (or quantization cell) associated with the observed \mathbf{x}_q as

$$\mathcal{S}(\mathbf{x}_q) \triangleq \{\boldsymbol{\theta} \in \Omega_{\boldsymbol{\theta}} : \mathbf{c}(\boldsymbol{\theta}) = \mathbf{x}_q\}, \quad (37)$$

i.e., the set of parameter values producing the same quantized output at high-SNR. Substituting (36) into (5) yields

$$p(\boldsymbol{\theta}|\mathbf{x}_a, \mathbf{x}_q) \xrightarrow{\text{SNR} \rightarrow \infty} \frac{p(\boldsymbol{\theta}) p(\mathbf{x}_a|\boldsymbol{\theta}) \mathbb{1}_{\{\boldsymbol{\theta} \in \mathcal{S}(\mathbf{x}_q)\}}}{\int_{\mathcal{S}(\mathbf{x}_q)} p(\boldsymbol{\theta}') p(\mathbf{x}_a|\boldsymbol{\theta}') d\boldsymbol{\theta}'}, \quad (38)$$

where $\mathbb{1}_A$ denotes the indicator of the event A . Thus, at high SNR levels, \mathbf{x}_q simply restricts the posterior support to $\mathcal{S}(\mathbf{x}_q)$; within this set, the posterior shape is governed solely by the prior $p(\boldsymbol{\theta})$ and the analog likelihood $p(\mathbf{x}_a|\boldsymbol{\theta})$. In particular, if the analog data is absent, the posterior reduces to the prior truncated to $\mathcal{S}(\mathbf{x}_q)$ and renormalized.

To characterize the non-monotonic MSE behavior in mixed-resolution systems, we partition the observation space into informative and saturation regimes. The latter is the event \mathcal{N} in which (36) holds, i.e., the signal lies in one cell. Under \mathcal{N} , \mathbf{x}_q becomes conditionally deterministic and conveys negligible information about $\boldsymbol{\theta}$. Thus, under \mathcal{N} , the estimation performance is dominated by the analog measurements. Using the law of total expectation, the MSE can be decomposed as

$$\begin{aligned} \text{MSE}(\hat{\boldsymbol{\theta}}) &= \mathbb{E} \left[(\hat{\boldsymbol{\theta}} - \boldsymbol{\theta})(\hat{\boldsymbol{\theta}} - \boldsymbol{\theta})^H | \mathcal{N} \right] \cdot \Pr(\mathcal{N}) \\ &\quad + \mathbb{E} \left[(\hat{\boldsymbol{\theta}} - \boldsymbol{\theta})(\hat{\boldsymbol{\theta}} - \boldsymbol{\theta})^H | \mathcal{N}^c \right] \cdot (1 - \Pr(\mathcal{N})), \end{aligned} \quad (39)$$

where \mathcal{N}^c denotes the complementary event of \mathcal{N} and $\Pr(\mathcal{N})$ can be evaluated as

$$\Pr(\mathcal{N}) = \mathbb{E}_{\boldsymbol{\theta}}[\Pr(\mathcal{N}|\boldsymbol{\theta})]. \quad (40)$$

Under the reasonable assumption that \mathbf{x}_a is informative enough, the indicator $\mathbb{1}_{\{\boldsymbol{\theta} \in \mathcal{S}(\mathbf{x}_q)\}}$ in (36) is redundant, and (38) can be approximated via the analog-only posterior $p(\boldsymbol{\theta}|\mathbf{x}_a)$, i.e., $p(\boldsymbol{\theta}|\mathbf{x}_a, \mathcal{N}) \xrightarrow{\text{SNR} \rightarrow \infty} p(\boldsymbol{\theta}|\mathbf{x}_a)$. Consequently, the MMSE estimator based on $(\mathbf{x}_a, \mathbf{x}_q)$ under \mathcal{N} approximately coincides with the MMSE estimator based only on \mathbf{x}_a , i.e.,

$$\hat{\boldsymbol{\theta}}_{\text{MMSE}}(\mathbf{x}_a, \mathbf{x}_q) \approx \hat{\boldsymbol{\theta}}_{\text{MMSE}}(\mathbf{x}_a), \quad \text{under } \mathcal{N},$$

where $\hat{\boldsymbol{\theta}}_{\text{MMSE}}(\mathbf{x}_a)$ is the MMSE estimator based solely on the analog data. Consequently, similar to (9), for the MMSE estimator we have

$$\begin{aligned} &\mathbb{E} \left[\mathbb{E} \left[(\hat{\boldsymbol{\theta}}_{\text{MMSE}}(\mathbf{x}_a, \mathbf{x}_q) - \boldsymbol{\theta}) \right. \right. \\ &\quad \times (\hat{\boldsymbol{\theta}}_{\text{MMSE}}(\mathbf{x}_a, \mathbf{x}_q) - \boldsymbol{\theta})^H | \mathbf{x}_a, \mathbf{x}_q, \mathcal{N} \Big] | \mathcal{N} \Big] \\ &\quad \approx \mathbb{E} \left[\mathbb{E} \left[(\hat{\boldsymbol{\theta}}_{\text{MMSE}}(\mathbf{x}_a) - \boldsymbol{\theta})(\hat{\boldsymbol{\theta}}_{\text{MMSE}}(\mathbf{x}_a) - \boldsymbol{\theta})^H | \mathbf{x}_a \right] \right]. \end{aligned} \quad (41)$$

To maintain analytical tractability, we further approximate the MMSE MSE in (41) using the closed-form MSE of the LMMSE estimator:

$$\begin{aligned} &\mathbb{E} \left[(\hat{\boldsymbol{\theta}}_{\text{MMSE}}(\mathbf{x}_a) - \boldsymbol{\theta})(\hat{\boldsymbol{\theta}}_{\text{MMSE}}(\mathbf{x}_a) - \boldsymbol{\theta})^H \right] \\ &\quad \approx \text{MSE}(\hat{\boldsymbol{\theta}}_{\text{LMMSE}}(\mathbf{x}_a)), \end{aligned} \quad (42)$$

where, similar to (11)-(12), the MSE of the analog-only LMMSE estimator is

$$\text{MSE}(\hat{\boldsymbol{\theta}}_{\text{LMMSE}}(\mathbf{x}_a)) = \boldsymbol{\Sigma}_{\boldsymbol{\theta}} - \mathbf{C}_{\boldsymbol{\theta}\mathbf{x}_a} \mathbf{C}_{\mathbf{x}_a}^{-1} \mathbf{C}_{\boldsymbol{\theta}\mathbf{x}_a}^H. \quad (43)$$

If the analog data is absent, the posterior in (38) is reduced to

$$p(\boldsymbol{\theta}|\mathbf{x}_q) \xrightarrow{\text{SNR} \rightarrow \infty} \frac{p(\boldsymbol{\theta}) \mathbb{1}_{\{\boldsymbol{\theta} \in \mathcal{S}(\mathbf{x}_q)\}}}{\int_{\mathcal{S}(\mathbf{x}_q)} p(\boldsymbol{\theta}') d\boldsymbol{\theta}'}. \quad (44)$$

Thus, instead of (43), the MSE of the MMSE estimator that is obtained from the posterior in (44) should be used.

In the informative region \mathcal{N}^c , the quantized observations have non-negligible variability, and we approximate the conditional MSE via the mixed-resolution WBCRB, as follows:

$$\mathbb{E}[(\hat{\boldsymbol{\theta}} - \boldsymbol{\theta})(\hat{\boldsymbol{\theta}} - \boldsymbol{\theta})^H | \mathcal{N}^c] \approx \text{WBCRB}. \quad (45)$$

The choice of weighting matrix in the WBCRB can be problem-specific; we adopt the selection in (28), which yields accuracy close to the optimal choice in our tests (Section VII).

By substituting the two approximations from (42) and (45) in (39), we obtain

$$\begin{aligned} \text{MSE}(\hat{\boldsymbol{\theta}}) &\approx \text{MSE}(\hat{\boldsymbol{\theta}}_{\text{LMMSE}}(\mathbf{x}_a)) \cdot \Pr(\mathcal{N}) \\ &\quad + \text{WBCRB} \cdot (1 - \Pr(\mathcal{N})). \end{aligned} \quad (46)$$

This approximation captures the transition in informativeness across the SNR range.

In general, the probability $\Pr(\mathcal{N})$ in (46) does not have closed-form expressions. We therefore adopt a lightweight Monte Carlo approach, similar to that used in Subsection III-B, as summarized in Algorithm 3. The computation in Algorithm 3 constitutes the main computational component of the proposed MSE approximation, and its complexity is dominated by data generation and equality checking of S \mathbf{x}_q samples, resulting in a per-sample cost of $\mathcal{O}(N_q S)$. This procedure is considerably more efficient than estimating the MSE of the MMSE estimator using Monte Carlo integration (see Algorithm 1), which requires computing high-dimensional conditional expectations for each sample and averaging the error. In addition, empirical results indicate that a modest number of iterations (e.g., $K = 10^2$ – 10^3) suffices for stable estimation of $\Pr(\mathcal{N}|\boldsymbol{\theta})$. Finally, for certain models, $\Pr(\mathcal{N}|\boldsymbol{\theta})$ admits a closed-form expression (see Subsection VI-C).

Algorithm 3: Monte Carlo Saturation Probability

Input:

- Distributions: $p(\boldsymbol{\theta})$, $p(\mathbf{x}_q|\boldsymbol{\theta})$
- Number of iterations: K
- Number of samples: S

Output: Estimated probability $\widehat{\Pr}(\mathcal{N})$

- 1: Initialize counter: $c_{\text{sat}} \leftarrow 0$
 - 2: **for** $k = 1, \dots, K$ **do**
 - 3: Draw the sample $\boldsymbol{\theta}^{(k)} \sim p(\boldsymbol{\theta})$
 - 4: Generate S i.i.d samples $\mathbf{x}_q^{(k,s)} \sim p(\mathbf{x}_q|\boldsymbol{\theta}^{(k)})$
 - 5: **if** $\mathbf{x}_q^{(k,s-1)} = \mathbf{x}_q^{(k,s)}$ **for all** $s = 2, \dots, S$ **then**
 - 6: $c_{\text{sat}} \leftarrow c_{\text{sat}} + 1$;
 - 7: **end for**
 - 7: $\widehat{\Pr}(\mathcal{N}) = c_{\text{sat}}/K$.
-

VI. LGO MODEL

In this section, we discuss the special case of parameter estimation with mixed-resolution data under the widely-used LGO model. In Subsection VI-A we present this model. The WBCRB from Section IV is developed for the LGO model in Subsection VI-B, and in Subsection VI-C we demonstrate the MSE approximation from Section V.

A. The LGO Model

In our previous work in [33], we showed that the following significant problems are special cases of the LGO model:

- Channel estimation in MIMO communication systems [33], [55], [58]–[60] (see Section V of [33]). An illustration of the MIMO system is shown in Fig. 2, where the parameter vector, θ , is estimated at the fusion center using the mixed-resolution data under the LGO model.
- Scalar parameter estimation, which is widely used in WSNs [1], [18] (see Section IV in [33]).
- Sequential linear models, where measurements are taken over time with the same system matrices, but with possibly different ADC resolutions (see Section V.A of [33]).

Tractable bounds can, hence, be used for these commonly used applications.

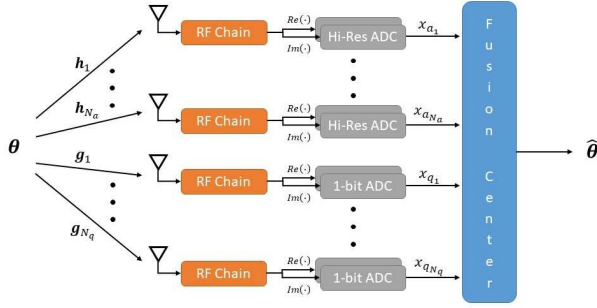


Fig. 2: Channel estimation with mixed-resolution measurements: a channel, θ , is estimated by transmitting a pilot sequence that is received by either high- or 1-bit low-resolution quantization. The unknown channel is estimated from the mixed-resolution measurements, \mathbf{x}_a , \mathbf{x}_q , in the fusion center.

Mathematically, the LGO model assumes:

- The parameter vector θ has a standard complex Gaussian distribution, $\theta \sim \mathcal{CN}(\mathbf{0}, \mathbf{I})$.
- The analog, high-resolution measurements satisfy

$$\mathbf{x}_a = \mathbf{H}\theta + \mathbf{u}_a, \quad (47)$$

where $\mathbf{H} = [\mathbf{H}_1^T, \mathbf{H}_2^T, \dots, \mathbf{H}_{N_a}^T]^T \in \mathbb{C}^{N_a \times M}$, in which

$$\mathbf{H}_n^H \mathbf{H}_n = \rho_a \mathbf{I}_M, \quad \forall n = 1, \dots, N_a, \quad (48)$$

$N_a = n_a M$, $\mathbf{u}_a \sim \mathcal{CN}(\mathbf{0}, \sigma_a^2 \mathbf{I}_{N_a})$, and $\sigma_a > 0$, $\rho_a > 0$ are known. If $i \neq j$, then $\mathbf{H}_i^H \mathbf{H}_j$ take arbitrary values. Thus, $\mathbf{x}_a | \theta \sim \mathcal{CN}(\mathbf{H}\theta, \sigma_a^2 \mathbf{I}_{N_a})$.

- The quantized, low-resolution measurements with a general threshold vector $\tau \in \mathbb{C}^{N_q}$ satisfy

$$\mathbf{x}_q = \mathcal{Q}(\mathbf{T}\theta + \mathbf{u}_q - \tau), \quad (49)$$

where $\mathbf{T} = \mathbf{1}_{N_q} \otimes \mathbf{T}_1 \in \mathbb{C}^{N_q \times M}$, in which $N_q = n_q M$, \otimes is the Kronecker product,

$$\mathbf{T}_1^H \mathbf{T}_1 = \rho_q \mathbf{I}_M, \quad (50)$$

$\mathbf{u}_q \sim \mathcal{CN}(\mathbf{0}, \sigma_q^2 \mathbf{I}_{N_q})$, and $\sigma_q > 0$, $\rho_q > 0$ are known. The operator $\mathcal{Q}(\cdot)$ is defined in (1). Under this model,

$$p(\mathbf{x}_q | \theta) = \prod_{n=1}^{N_q} \Phi(\zeta_n^R)^{\left(\frac{1}{2} + \frac{\text{Re}\{\mathbf{x}_{q_n}\}}{\sqrt{2}}\right)} (1 - \Phi(\zeta_n^R))^{\left(\frac{1}{2} - \frac{\text{Re}\{\mathbf{x}_{q_n}\}}{\sqrt{2}}\right)} \times \Phi(\zeta_n^I)^{\left(\frac{1}{2} + \frac{\text{Im}\{\mathbf{x}_{q_n}\}}{\sqrt{2}}\right)} (1 - \Phi(\zeta_n^I))^{\left(\frac{1}{2} - \frac{\text{Im}\{\mathbf{x}_{q_n}\}}{\sqrt{2}}\right)}, \quad (51)$$

where $\phi(\cdot)$ and $\Phi(\cdot)$ denote the standard Gaussian PDF and CDF, respectively.

- The noise vectors, \mathbf{u}_a and \mathbf{u}_q , and the parameters in θ are assumed to be mutually independent.

The details on numerically computing the LMMSE and MMSE estimators under this model can be found in [31]. In particular, by substituting the prior and data probability functions (51) in Algorithm 1 we obtain the MMSE estimator. In addition, it should be noted that for the case where $\tau = \mathbf{0}$, the LMMSE estimator has a closed-form expression [33].

B. WBCRB

We demonstrated in (20) that for the specified model, the BFIM can be decomposed into prior, analog, and quantized contributions. Under the LGO model, this decomposition takes the form given in [31, Eq. (17)]:

$$\mathbf{J} = \mathbf{I}_M + \frac{1}{\sigma_a^2} \mathbf{H}^H \mathbf{H} + \frac{1}{2\sigma_q^2} \mathbf{T}^H \mathbb{E}_\theta[\mathbf{D}(\theta)] \mathbf{T}, \quad (52)$$

where \mathbf{T} is defined before (50) and $\mathbf{D}(\theta) = \text{diag}([d_1(\theta), \dots, d_{N_q}(\theta)]) \in \mathbb{R}^{N_q \times N_q}$, in which

$$d_n(\theta) \triangleq \frac{\phi^2(\zeta_n^R)}{\Phi(\zeta_n^R)\Phi(-\zeta_n^R)} + \frac{\phi^2(\zeta_n^I)}{\Phi(\zeta_n^I)\Phi(-\zeta_n^I)}, \quad (53)$$

$$\zeta_n^R \triangleq \frac{\sqrt{2}}{\sigma_q} \text{Re}\{\mathbf{t}_n^T \theta - \tau_n\}, \quad \zeta_n^I \triangleq \frac{\sqrt{2}}{\sigma_q} \text{Im}\{\mathbf{t}_n^T \theta - \tau_n\}, \quad (54)$$

and $\mathbf{t}_n \in \mathbb{C}^{M \times 1}$ is the n th row of \mathbf{T} .

We next examine the special cases from Subsection IV-C

1) *BCRB*: The BCRB from Subsection IV-C1 for this case is given by the inverse of (52), which also has a closed-form solution without requiring matrix inversion [31]. As shown in [51, p. 7], the BCRB is asymptotically tight iff the posterior BFIM, $\mathbf{J}_{\mathbf{x}|\theta}$, is independent of θ . However, from (52) it can be seen that the quantized component of the BFIM, $\mathbf{J}_{\mathbf{x}_q|\theta}$, depends on θ . Consequently, the BCRB is not asymptotically tight in this case, which highlights the need for an alternative bound. Moreover, in [31] we showed the limitation of the BCRB for the LGO model, which does not capture the non-monotonic behavior of the MSE w.r.t. SNR in this case.

2) *FIM-Inverse Weighting*: For this bound from Subsection IV-C2, similar to the derivation of (52), it can be shown that (28) under the LGO model is reduced to

$$\mathbf{W}(\theta) = \left(\theta \theta^H + \frac{1}{\sigma_a^2} \mathbf{H}^H \mathbf{H} + \frac{1}{2\sigma_q^2} \mathbf{T}^H \mathbf{D}(\theta) \mathbf{T} \right)^{-1}. \quad (55)$$

To compute \mathbf{G} in this case, we compute the derivatives of (55) by using known derivative rules (see, e.g., [61, eq. 3.40]) as follows:

$$\frac{\partial [\mathbf{W}(\theta)]_{k,m}}{\partial \theta_m^*} = -[\mathbf{W}(\theta) \times \left(\theta \mathbf{e}_m^T + \frac{n_q}{2\sigma_q^2} \sum_{n=1}^M \frac{\partial(d_n(\theta))}{\partial \theta_m^*} \mathbf{t}_n^* \mathbf{t}_n^T \right) \mathbf{W}(\theta)^H]_{k,m}, \quad (56)$$

$k, m = 1, \dots, M$, for $\mathbf{W}(\theta)$ from (55), where $\mathbf{e}_m \in \mathbb{R}^M$ is the m th column of the $M \times M$ identity matrix. In particular, for the scalar case ($M = 1$), (56) is reduced to

$$\frac{dw(\theta)}{d\theta^*} = -w(\theta)^2 \left(\theta + \frac{n_q \rho_q}{2\sigma_q^2} \frac{d(d(\theta))}{d\theta^*} \right), \quad (57)$$

where we used (50). The regularity conditions from Section IV are satisfied in this case too.

It should be noted that, similar to the BCRB, obtaining a closed-form expression for the WBCRB requires numerically evaluating the expectation (w.r.t. $\boldsymbol{\theta}$) of the diagonal matrix $\mathbf{D}(\boldsymbol{\theta})$, as well as the derivatives $\frac{\partial d_n(\boldsymbol{\theta})}{\partial \theta_n^*}$. This evaluation can be carried out using numerical integration. Nevertheless, the computation of this bound is significantly less demanding than computing the MMSE estimator from Subsection III-A, as it avoids two-dimensional integration and does not require integration over the likelihood function or generating observations $[\mathbf{x}_a, \mathbf{x}_q]$. This reduces the complexity from high-dimensional integration to a tractable $\mathcal{O}(K)$ procedure, where K is the number of Monte Carlo simulations, making it feasible even for large N_q . In the supplemental material attached to this paper, we show that under the LGO model there is no need to develop an augmented version of this bound.

Recalling that an asymptotically tight bound occurs iff $\mathbf{J}_{\mathbf{x}|\boldsymbol{\theta}}$ in (19) is independent of $\boldsymbol{\theta}$ (see Section IV-C2), and applying (55) while neglecting the prior FIM, we obtain

$$\mathbf{J}_{\mathbf{x}|\boldsymbol{\theta}}(\boldsymbol{\theta}) = \frac{1}{\sigma_a^2} \mathbf{H}^H \mathbf{H} + \frac{1}{2\sigma_q^2} \mathbf{T}^H \mathbf{D}(\boldsymbol{\theta}) \mathbf{T}. \quad (58)$$

Since $\mathbf{J}_{\mathbf{x}|\boldsymbol{\theta}}$ depends on $\boldsymbol{\theta}$ in the presence of 1-bit data, the BCRB is not asymptotically tight here, which explains the motivation for a tighter bound, such as the proposed WBCRB.

C. MSE Approximation

In this subsection, we derive a closed-form expression for the conditional probability of the event \mathcal{N} (in which (36) holds) under the LGO model. This enables replacing the empirical approximation used in Algorithm 3 with a semi-analytical computation.

Recall that \mathcal{N} denotes the event in which all quantized measurements lie within a single cell. Under the LGO model, and specifically, (49), $\mathbf{c}(\boldsymbol{\theta})$ from (37) is given by

$$\mathbf{c}(\boldsymbol{\theta}) = \mathcal{Q}(\mathbf{T}\boldsymbol{\theta} - \boldsymbol{\tau}). \quad (59)$$

Thus,

$$\Pr(\mathcal{N}) = \Pr(\mathcal{Q}(\mathbf{T}\boldsymbol{\theta} + \mathbf{u}_q - \boldsymbol{\tau}) = \mathcal{Q}(\mathbf{T}\boldsymbol{\theta} - \boldsymbol{\tau})). \quad (60)$$

Note that if $\boldsymbol{\tau}$ is block-replicated as $\boldsymbol{\tau} = \mathbf{1}_{n_q} \otimes \boldsymbol{\tau}_1$, then $\mathbf{c}(\boldsymbol{\theta}) = \mathbf{1}_{n_q} \otimes \mathcal{Q}(\mathbf{T}_1 \boldsymbol{\theta} - \boldsymbol{\tau}_1)$. Conditioned on $\boldsymbol{\theta}$, consider each component n of the quantized measurement. Under the LGO model, the noise $u_{q,n} \sim \mathcal{CN}(0, \sigma_q^2)$ so that $\Re\{u_{q,n}\}, \Im\{u_{q,n}\} \stackrel{\text{i.i.d.}}{\sim} \mathcal{N}(0, \sigma_q^2/2)$. With the 1-bit quantizer in (1), the real (resp. imaginary) output equals $+\frac{1}{\sqrt{2}}$ iff the noisy real (resp. imaginary) input is ≥ 0 , and $-\frac{1}{\sqrt{2}}$ otherwise. Hence, the “no sign flip” events are

$$\text{sign}(\Re\{\mathbf{t}_n^T \boldsymbol{\theta} - \tau_n + u_{q,n}\}) = \text{sign}(\Re\{\mathbf{t}_n^T \boldsymbol{\theta} - \tau_n\}),$$

$$\text{sign}(\Im\{\mathbf{t}_n^T \boldsymbol{\theta} - \tau_n + u_{q,n}\}) = \text{sign}(\Im\{\mathbf{t}_n^T \boldsymbol{\theta} - \tau_n\}).$$

Using standard Gaussian tail relations, under the LGO model, the corresponding conditional probabilities (for the two outcomes per part) are

$$\Pr\left(\Re\{x_{q,n}\} = \pm \frac{1}{\sqrt{2}} \mid \boldsymbol{\theta}\right) = \Phi(\pm \zeta_n^R), \quad (61)$$

$$\Pr\left(\Im\{x_{q,n}\} = \pm \frac{1}{\sqrt{2}} \mid \boldsymbol{\theta}\right) = \Phi(\pm \zeta_n^I), \quad (62)$$

where ζ_n^R, ζ_n^I are defined in (54). Using conditional independence across n and between real and imaginary parts given $\boldsymbol{\theta}$, the conditional probability that all quantized measurements match their noiseless decision cell is

$$\begin{aligned} \Pr(\mathcal{N}|\boldsymbol{\theta}) &= \prod_{n=1}^{N_q} \Pr(\text{no flip in real}|\boldsymbol{\theta}) \Pr(\text{no flip in imag}|\boldsymbol{\theta}) \\ &= \prod_{n=1}^{N_q} \Phi(|\zeta_n^R|) \Phi(|\zeta_n^I|). \end{aligned} \quad (63)$$

Finally, by substituting (63) in (40), we obtain

$$\Pr(\mathcal{N}) = \mathbb{E}_{\boldsymbol{\theta}} \left[\prod_{n=1}^{N_q} \Phi(|\zeta_n^R|) \times \Phi(|\zeta_n^I|) \right], \quad (64)$$

where (64) computed by averaging over the prior distribution of $\boldsymbol{\theta}$. In practice, this is implemented via Monte Carlo simulations w.r.t. the prior of $\boldsymbol{\theta}$, and reduces the problem to sampling over $\boldsymbol{\theta}$, rather than evaluating estimator performance. Importantly, in the high-SNR regime where $\sigma_q \rightarrow 0$, whenever $\Re\{\mathbf{t}_n^T \boldsymbol{\theta} - \tau_n\}$ or $\Im\{\mathbf{t}_n^T \boldsymbol{\theta} - \tau_n\}$ is nonzero, we have $\Phi(|\zeta_n^R|), \Phi(|\zeta_n^I|) \rightarrow 1$, hence the overall probability $\Pr(\mathcal{N})$ converges to 1; the measure-zero case of exactly zero mean does not alter the integral under a continuous prior. This behavior formally captures the saturation effect of quantized measurements: at sufficiently high SNR, all quantized outputs collapse to a deterministic constant value, so that $\Pr(\mathcal{N}) \rightarrow 1$, and the quantized data become asymptotically uninformative compared to the analog data.

Remark: For a pure 1-bit system, $n_a = 0$, it can be shown based on (44), that the MSE of the LMMSE and MMSE estimators converge to [45]

$$\lim_{\sigma_q \rightarrow 0} \text{MSE}(\hat{\boldsymbol{\theta}}_{\text{MMSE}}(\mathbf{x}_q)) = (1 - \frac{2}{\pi}) \mathbf{I}_M. \quad (65)$$

By substituting (64), (65), and the WBCRB into (46), we obtain the MSE approximation for this case.

VII. SIMULATIONS

In this section, we evaluate the proposed bounds and the MSE approximation method under the LGO model described in Section VI. We compare them with the MSE of the MMSE and LMMSE estimators. The MMSE estimator is implemented using Algorithm 1. The LMMSE estimator is implemented using the closed-form expression from [33] for $\boldsymbol{\tau} = 0$, and via Algorithm 1 in [31] for general threshold values. The simulations are performed for the scalar case $M = 1$, which enables feasible implementation of the MMSE estimator.

The following performance analysis tools are examined:

- The BCRB from (27), which, under the LGO model, is given by the inverse of (52), computed without matrix inversion as in [31].
- The WBCRB based on the FIM-inverse weighting from Subsection IV-C2, computed under the LGO model using (55), denoted as “WBCRB”.
- The optimal WBCRB, obtained from (35) with $\Delta = 0.2$ and $L = 1,000$ test points, denoted as “WBCRB opt”.
- The proposed MSE approximation method (46), where the saturation regime probability is computed using (64).

Unless stated otherwise, all results are obtained by 1000 Monte Carlo trials, with parameters $\sigma_a^2 = \sigma_q^2 = \sigma^2$, $\rho_a = \rho_q = 1$, $N_t = 1,000$, and $M = 1$, where $\text{SNR} \triangleq \rho/\sigma$.

A. Test Case 1: Effect of the Threshold

In Figs. 3a and 3b, we present the MSE of the MMSE and LMMSE estimators, along with the different bounds, versus SNR for $n_a = 1$, $n_q = 100$, and two threshold settings: $\tau = 0$ (Fig. 3a) and $\tau = 2.5$ (Fig. 3b). In both cases, the MSE curves exhibit non-monotonic dependence on SNR, reflecting the varying informativeness of the quantized measurements. For $\tau = 0$ (Fig. 3a), the BCRB decreases monotonically with SNR and fails to capture the region where the quantized data becomes non-informative. For $\tau = 2.5$ (Fig. 3b), the BCRB itself exhibits non-monotonic behavior, providing a better qualitative match to the estimator MSE trends. However, in this case the overall MSE is significantly higher, making such thresholds undesirable from a performance standpoint. These results reveal a trade-off: the BCRB is tighter when estimator performance is degraded, which emphasizes the need for tighter bounds. In addition, it can be seen that the FIM-inverse weighting WBCRB and the optimal WBCRB exhibit non-monotonic behavior and track the different regions of the MSE of the estimators with high accuracy. In Fig. 3a, the FIM-inverse weighting WBCRB is close to the optimal WBCRB, which makes it a more practical choice in this setting. The proposed MSE approximation method further improves prediction accuracy for both cases, and closely matches the MMSE performance. At high SNR, all estimators and bounds converge, as the estimation relies solely on the analog observations under Gaussian noise. Regarding the MSE approximation, when $\tau \approx 0$, the proposed method is tighter than the WBCRB, and closely matches the MMSE estimator.

Figure 4 complements this analysis by showing the MSE and bounds as a function of the quantization threshold τ for $\sigma = 1/2$ and $(n_a, n_q) = (1, 100)$. As τ increases, the system approaches the saturation region, in which most quantized outputs collapse to identical values, leading to saturation in both the MSE and the WBCRB variants. In the mid-threshold region of $\tau \in [0.5, 2]$, the FIM-inverse weighting WBCRB is significantly tighter and follows the MMSE more closely than the conventional BCRB, highlighting its advantage in accurately capturing estimation performance in transition regions between informative and non-informative quantized measurements.

B. Test Case 2: 1-Bit System

In Fig. 5, we present the MSE of the LMMSE and MMSE estimators versus SNR for different values of n_q (20 and 40), under a pure 1-bit system ($n_a = 0$) and $\tau = 0$. The optimal WBCRB is omitted for clarity, as its behavior closely matches that of FIM-inverse weighting WBCRB in this case. It can be seen that as the SNR increases, the performance of both estimators converges to a constant value, which is independent of n_q , consistent with the saturation phenomenon discussed in Sections V and VI-C. This behavior arises from the loss of information in quantized measurements at high SNR (cf. event \mathcal{N} (36)). The BCRB fails to reflect this trend, decreases monotonically with SNR, and maintains an artificial gap between different sensor configurations ($n_q = 20$ and $n_q = 40$) even asymptotically. In contrast, the WBCRB captures the non-monotonic behavior and the convergence of performance across n_q values in the high-SNR regime, although it is not a tight bound. Notably, the proposed MSE

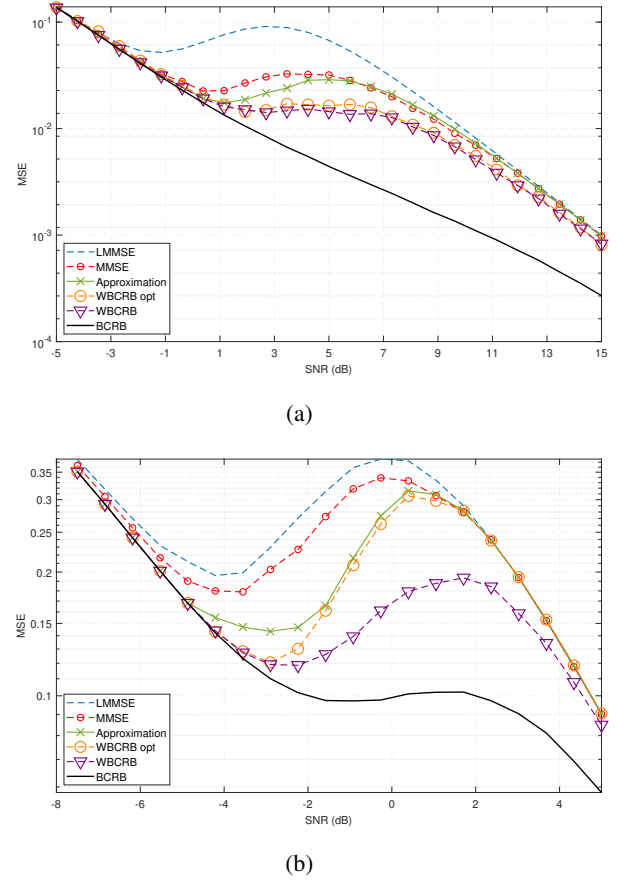


Fig. 3: MSE of the MMSE and LMMSE estimators in comparison to different WBCRB weight selection versus SNR for $(n_a, n_q) = (1, 100)$ and (a) $\tau = 0$ (b) $\tau = 2$.

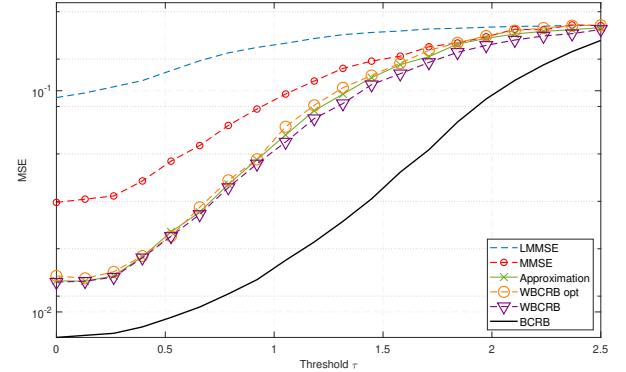


Fig. 4: MSE of the MMSE and LMMSE estimators in comparison to different WBCRB weight selection versus τ for $(n_a, n_q) = (1, 100)$ and $\sigma = \frac{1}{2}$

approximation almost perfectly matches the MMSE curve over the entire SNR range and converges to the theoretical limit $1 - \frac{2}{\pi}$ at high SNR (see (65)). This figure thus highlights the importance of the proposed approximation method as a reliable and computationally efficient tool for accurately predicting estimation performance when quantization is involved.

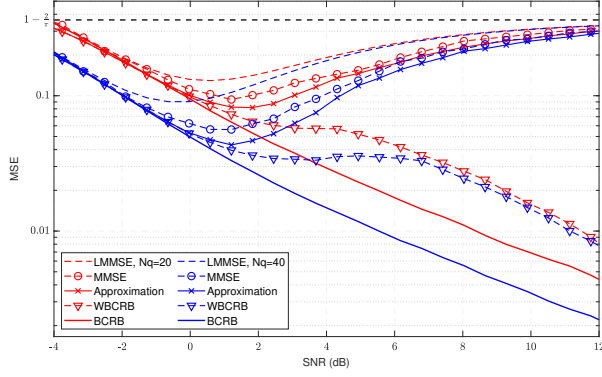


Fig. 5: MSE of the LMMSE and MMSE estimators in comparison with WBCRB and BCRB versus SNR for different pure 1-bit partitions, $n_a = 0$, and $\tau = 0$.

C. Resource Allocation

We next examine the use of the proposed MSE approximation (VI-C) as a practical design tool for resource allocation between analog and quantized measurements in mixed-resolution systems. Resource allocation plays a central role in determining the performance–power trade-off, as the partition (n_a, n_q) directly impacts estimation accuracy across different SNR regimes. Figure 6 shows the MSE of the estimators, the proposed MSE approximation, and the mixed-resolution BCRB for two measurement partitions: $(n_a, n_q) = (1, 150)$ and $(n_a, n_q) = (2, 100)$. While the MMSE curves reveal that the optimal partition depends on the SNR, with an intersection at $\text{SNR} \approx 2.5$, and analog-heavy configurations outperforming at high SNR, the BCRB fails to capture these trends. In particular, at high SNR the BCRB reveals no change in relative performance, even though quantized data becomes non-informative and the number of analog measurements dominates accuracy. In contrast, the WBCRB, used as the basis for the proposed approximation, captures the impact of the quantized data, enabling a more accurate prediction of performance trends than the BCRB. Moreover, the proposed MSE approximation, which builds on the WBCRB from (55), closely tracks the MMSE across all SNR regions and correctly identifies the more effective partition in each region, with intersection at $\text{SNR} \approx 5$ (as predicted by the WBCRB). This figure thus highlights the proposed approximation as a reliable tool for mixed-resolution system design.

VIII. CONCLUSIONS

In this paper, we developed the WBCRB for mixed-resolution Bayesian estimation using both quantized and analog data. Several weighting strategies were investigated, including the conventional BCRB, a data-aware WBCRB based on the inverse instantaneous BFIM, and the optimal WBCRB [32]. We also proposed an SNR-dependent MSE approximation method that partitions the parameter space according to the informativeness of the quantized measurements, expressing the overall MSE as a weighted combination of region-specific WBCRBs and an analog-only estimator. As an illustrative case, the WBCRBs and MSE approximation were derived for the widely used LGO model. Simulation results

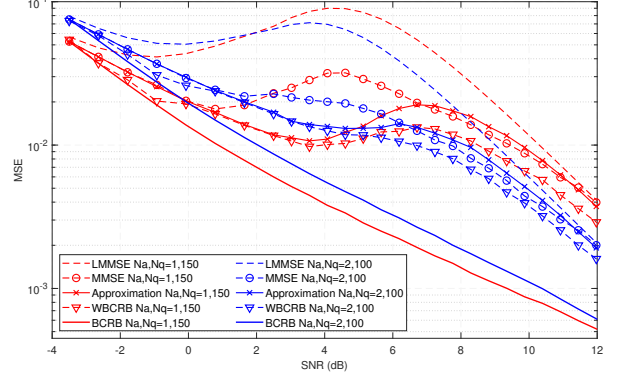


Fig. 6: The MSE of the BCRB and MMSE estimator in comparison with the proposed MSE approximation as a function of the SNR for different numbers of measurements.

showed that the proposed WBCRB variants closely track the MSE of the MMSE estimator, substantially outperforming the BCRB. The improvement is most pronounced in the mid-SNR region, where quantization effects lead to non-monotonic MSE behavior: while the BCRB fails to capture these transitions, the two WBCRBs reliably predict them. The SNR-dependent MSE approximation further demonstrates even higher accuracy compared to the bounds, offering a practical performance prediction tool. Overall, the results highlight the value of the WBCRB framework for accurate performance analysis and resource allocation in mixed-resolution systems.

APPENDIX A PROOF OF THEOREM 1

The proof is along the lines of the proof in [32], adapted for the mixed-resolution setting, e.g., it explicitly incorporates summations for the quantized data. For simplicity, in this appendix we denote an arbitrary estimator of θ by $\hat{\theta}(\mathbf{x}_a, \mathbf{x}_q)$.

Step 1 - Definition of the Auxiliary Function: Let the vector function $\mathbf{g}(\mathbf{x}_a, \mathbf{x}_q, \theta) \in \mathbb{C}^M$ be

$$\mathbf{g}(\mathbf{x}_a, \mathbf{x}_q, \theta) = \mathbf{W}(\theta) \nabla_{\theta}^H \{ \log p(\theta) p(\mathbf{x}_a | \theta) p(\mathbf{x}_q | \theta) \} + \mathbf{v}(\theta), \quad (66)$$

where the elements of $\mathbf{v}(\theta)$ are defined in (21). According to Condition 1 and the differentiability of $\mathbf{W}(\theta)$, $\mathbf{g}(\mathbf{x}_a, \mathbf{x}_q, \theta)$ is well-defined and is differentiable w.r.t. θ . Next, we verify that it satisfies the crucial unbiasedness property [50], [51]:

$$\mathbb{E}_{\theta | \mathbf{x}_a, \mathbf{x}_q} [\mathbf{g}(\mathbf{x}_a, \mathbf{x}_q, \theta) | \mathbf{x}_a, \mathbf{x}_q] = \mathbf{0}. \quad (67)$$

For each k , we have

$$\begin{aligned} & \mathbb{E}_{\theta | \mathbf{x}_a, \mathbf{x}_q} [g_k^*(\mathbf{x}_a, \mathbf{x}_q, \theta) | \mathbf{x}_a, \mathbf{x}_q] \\ &= \int_{\Omega_{\theta}} \sum_{m=1}^M \left([\mathbf{W}^*(\theta)]_{k,m} \frac{\partial \log(p(\cdot))}{\partial \theta_m} + \frac{\partial [\mathbf{W}^*(\theta)]_{k,m}}{\partial \theta_m} \right) p(\theta | \mathbf{x}_a, \mathbf{x}_q) d\theta. \end{aligned} \quad (68)$$

Using the derivative of the log and interchanging the order of summing and integration (see Condition 2), one obtains

$$\begin{aligned} & \mathbb{E}_{\theta|\mathbf{x}_a, \mathbf{x}_q} [g_k^*(\mathbf{x}_a, \mathbf{x}_q, \theta) | \mathbf{x}_a, \mathbf{x}_q] \\ &= \sum_{m=1}^M \int_{\Omega_{\theta}} \frac{\partial [\mathbf{W}^*(\theta)]_{k,m}}{\partial \theta_m} p(\theta | \mathbf{x}_a, \mathbf{x}_q) d\theta \\ &+ \sum_{m=1}^M \int_{\Omega_{\theta}} [\mathbf{W}^*(\theta)]_{k,m} \frac{\partial p(\theta | \mathbf{x}_a, \mathbf{x}_q)}{\partial \theta_m} d\theta \\ &= \sum_{m=1}^M \int_{\Omega_{\theta}} \frac{\partial}{\partial \theta_m} ([\mathbf{W}^*(\theta)]_{k,m} p(\theta | \mathbf{x}_a, \mathbf{x}_q)) d\theta. \end{aligned} \quad (69)$$

Applying integration by parts to the last term, and using (14a), the boundary terms vanish and we get (67). Thus, the vector-valued function $\mathbf{g}(\mathbf{x}_a, \mathbf{x}_q, \theta)$ is properly constructed for use in the Cauchy-Schwarz-based bound derivation in the following.

Step 2 - Cauchy-Schwarz inequality and derivation of (23): Let $\hat{\theta}$ be any estimator of θ . Using the Cauchy-Schwarz inequality [51, Eq. (189)], the MSE matrix satisfies

$$\mathbb{E}[(\hat{\theta} - \theta)(\hat{\theta} - \theta)^H] \succeq \mathbb{E}[(\hat{\theta} - \theta) \mathbf{g}^H(\mathbf{x}_a, \mathbf{x}_q, \theta)] \times \tilde{\mathbf{G}}^{-1} \mathbb{E}[\mathbf{g}(\mathbf{x}_a, \mathbf{x}_q, \theta)(\hat{\theta} - \theta)^H], \quad (70)$$

where

$$\tilde{\mathbf{G}} = \mathbb{E}[\mathbf{g}(\mathbf{x}_a, \mathbf{x}_q, \theta) \mathbf{g}^H(\mathbf{x}_a, \mathbf{x}_q, \theta)]. \quad (71)$$

It should be noted that we use the fact that, according to (2) $\mathbf{g}(\mathbf{x}, \theta)$ in (66) is a measurable function that satisfies (67), and thus, the use of (70) is valid [51].

Substituting $\mathbf{g}(\mathbf{x}_a, \mathbf{x}_q, \theta)$ from (66) in (23), results in

$$\begin{aligned} \tilde{\mathbf{G}} &= \mathbb{E}[\mathbf{W}(\theta) \nabla_{\theta}^H \log p(\cdot) \nabla_{\theta} \log p(\cdot) \mathbf{W}^H(\theta)] \\ &+ \mathbb{E}[\mathbf{W}(\theta) \nabla_{\theta}^H \log p(\cdot) \mathbf{v}^H(\theta)] \\ &+ \mathbb{E}[\mathbf{v}(\theta) \nabla_{\theta} \log p(\cdot) \mathbf{W}^H(\theta)] \\ &+ \mathbb{E}[\mathbf{v}(\theta) \mathbf{v}^H(\theta)], \end{aligned} \quad (72)$$

where in this appendix $p(\cdot)$ is used as a shorthand for $p(\theta)p(\mathbf{x}_a|\theta)p(\mathbf{x}_q|\theta)$. Using Condition 4, the (n, k) th element of the third term in (72) can be written as

$$\begin{aligned} & \mathbb{E}[v_n(\theta) [\nabla_{\theta} \log p(\theta) \mathbf{W}^H(\theta)]_k] \\ &= \mathbb{E}\left[\sum_{m=1}^M \mathbf{W}^*(\theta)_{k,m} \frac{\partial \log p(\theta)}{\partial \theta_m} v_n(\theta)\right] \\ &= \sum_{m=1}^M \int_{\Omega_{\theta}} \frac{\partial p(\theta)}{\partial \theta_m} [\mathbf{W}(\theta)]_{k,m}^* v_n(\theta) d\theta, \end{aligned} \quad (73)$$

where the sum and integration may be interchanged under Condition 2. Using integration by parts for the inner expression and using the condition in (14b), we obtain that each marginal integral in (73) satisfies

$$\begin{aligned} & \int_{[\Omega_{\theta}]_m} \frac{\partial p(\theta)}{\partial \theta_m} [\mathbf{W}(\theta)]_{k,m}^* v_n(\theta) d\theta \\ &= - \int_{[\Omega_{\theta}]_m} \frac{\partial ([\mathbf{W}(\theta)]_{k,m}^* v_n(\theta))}{\partial \theta_m} p(\theta) d\theta. \end{aligned} \quad (74)$$

Substitution of (74) into (73) results in

$$\mathbb{E}[v_n(\theta) [\nabla_{\theta} \log p(\theta) \mathbf{W}^H(\theta)]_k] = [\mathbf{A}]_{k,n}^*, \quad (75)$$

where the elements of \mathbf{A} are defined in (22). Similarly, the second term in (72) equals \mathbf{A} . Substituting these results in (72), we obtain $\tilde{\mathbf{G}} = \mathbf{G}$, where \mathbf{G} is defined in (23). Note that this derivation of \mathbf{A} leads to an expression for \mathbf{G} that depends solely on the weight matrix $\mathbf{W}(\theta)$.

Step 3 - Evaluation of the Mixed Term: To complete the proof, we need to compute the cross-moment in (70). First, using (66) one obtains

$$\begin{aligned} \mathbb{E}[(\hat{\theta} - \theta) \mathbf{g}^H(\mathbf{x}_a, \mathbf{x}_q, \theta)] &= \int \sum_{\mathbf{x}_q \in \mathcal{Z}^{N_q}} \int_{\mathbb{C}^{N_a}} (\hat{\theta} - \theta) \\ &\times (\mathbf{W}(\theta) \nabla_{\theta}^H \log p(\cdot) + \mathbf{v}(\theta)) p(\cdot) d\mathbf{x}_a d\theta, \end{aligned} \quad (76)$$

where the interchange of sum and integral is justified by Condition 2. The (n, k) th element of this matrix is given by

$$\begin{aligned} & \mathbb{E}[(\hat{\theta}_n - \theta_n) g_k^*(\mathbf{x}_a, \mathbf{x}_q, \theta)] \\ &= \sum_{\mathbf{x}_q \in \mathcal{Z}^{N_q}} \int_{\mathbb{C}^{N_a}} \sum_{m=1}^M \int_{\Omega_{\theta}} (\hat{\theta}_n - \theta_n) \\ &\times [\mathbf{W}^*(\theta)]_{k,m} \frac{\partial \log p(\cdot)}{\partial \theta_m} + \frac{\partial [\mathbf{W}^*(\theta)]_{k,m}}{\partial \theta_m} p(\cdot) d\theta d\mathbf{x}_a \\ &= \sum_{\mathbf{x}_q \in \mathcal{Z}^{N_q}} \int_{\mathbb{C}^{N_a}} \sum_{m=1}^M \int_{\Omega_{\theta}} (\hat{\theta}_n - \theta_n) \\ &\times [\mathbf{W}^*(\theta)]_{k,m} \frac{\partial p(\cdot)}{\partial \theta_m} + p(\cdot) \frac{\partial [\mathbf{W}^*(\theta)]_{k,m}}{\partial \theta_m} d\theta d\mathbf{x}_a. \end{aligned} \quad (77)$$

Integration by parts over θ_m on the r.h.s. in (77) yields

$$- \int \delta_{n,m} [\mathbf{W}^*(\theta)]_{k,m} p(\theta) p(\mathbf{x}_a|\theta) p(\mathbf{x}_q|\theta) d\theta, \quad (78)$$

where $\delta_{n,m}$ is the Kronecker delta, and due to (14a), the boundary terms vanish. It should be noted that we used the fact that for any differentiable function $f(\theta)$,

$$\theta_n \frac{\partial f(\theta)}{\partial \theta_m} = \frac{\partial}{\partial \theta_m} \{\theta_n f(\theta)\} - \delta_{n,m} f(\theta).$$

By substituting (78) in (76), and using the fact that $\mathbf{W}(\theta)$ is a Hermitian matrix, we obtain

$$\mathbb{E}[(\hat{\theta} - \theta) \mathbf{g}^H(\mathbf{x}_a, \mathbf{x}_q, \theta)] = -\mathbb{E}[\mathbf{W}^H(\theta)]. \quad (79)$$

By substituting $\tilde{\mathbf{G}} = \mathbf{G}$ (see after (75)), (75), and (79) in (70), we obtain the WBCRB in (24).

REFERENCES

- [1] A. Ribeiro and G. B. Giannakis, "Bandwidth-constrained distributed estimation for wireless sensor networks-part I: Gaussian case," *IEEE Trans. Signal Processing*, vol. 54, no. 3, pp. 1131–1143, 2006.
- [2] S. Yusuf and C. Cagatay, "A feedback quantization scheme leveraging fairness and throughput for heterogeneous multi-user diversity systems," *IEEE Trans. Veh. Technol.*, vol. 59, no. 5, pp. 2610–2614, 2010.
- [3] L. Xu, F. Gao, T. Zhou, S. Ma, and W. Zhang, "Joint channel estimation and mixed-ADCs allocation for massive MIMO via deep learning," *IEEE Trans. Wireless Communications*, vol. 22, no. 2, pp. 1029–1043, 2022.
- [4] A. Ribeiro and G. Giannakis, "Bandwidth-constrained distributed estimation for wireless sensor networks-part II: Unknown probability density function," *IEEE Trans. Signal Processing*, vol. 54, no. 7, pp. 2784–2796, 2006.
- [5] A. Ribeiro, I. D. Schizas, S. I. Roumeliotis, and G. Giannakis, "Kalman filtering in wireless sensor networks," *IEEE Control Systems*, vol. 30, no. 2, pp. 66–86, 2010.
- [6] H. Chen, T. Kirubarajan, and Y. Bar-Shalom, "Tracking of spawning targets with multiple finite resolution sensors," *IEEE Trans. Aerospace and Electronic Systems*, vol. 44, no. 1, 2008.

- [7] H. Pirzadeh and A. L. Swindlehurst, "Spectral efficiency of mixed-ADC massive MIMO," *IEEE Trans. Signal Processing*, vol. 66, no. 13, pp. 3599–3613, 2018.
- [8] X. Zhang, Y. Cheng, X. Shang, J. Liu, "CRB Analysis for Mixed-ADC Based DOA Estimation," *IEEE Trans. Signal Processing*, vol. 72, pp. 3043–3058, 2024.
- [9] N. Liang and W. Zhang, "Mixed-ADC massive MIMO," *IEEE J. Sel. Areas Commun.*, vol. 34, no. 4, pp. 983–997, 2016.
- [10] D. Abdelhameed, K. Umebayashi, I. Atzeni, and A. Tölli, "Enhanced signal detection and constellation design for massive SIMO communications with 1-bit ADCs," *IEEE Access*, pp. 11 749–11 765, 2023.
- [11] B. Fesl and W. Utschick, "Linear and nonlinear MMSE estimation in one-bit quantized systems under a Gaussian mixture prior," *IEEE Signal Processing Letters*, vol. 32, pp. 361–365, 2025.
- [12] Y. Cho, J. Choi, B.L. Evans, "Learning-based one-bit maximum likelihood detection for massive mimo systems: Dithering-aided adaptive approach," *IEEE Trans. Veh. Technol.*, vol. 73, pp. 11 680–11 693, 2024.
- [13] Mark D. McDonnell, Nigel G. Stocks, Charles E. M. Pearce, and Derek Abbott, *Stochastic Resonance*. Cambridge University Press, 2008.
- [14] H. Fu, Y. Chi, "Quantized spectral compressed sensing: Cramér–Rao bounds and recovery algorithms," *IEEE Trans. on Signal Processing*, vol. 66, pp. 3268–3279, 2018.
- [15] P. Stoica, X. Shang, and Y. Cheng, "The Cramér–Rao bound for signal parameter estimation from quantized data [lecture notes]," *IEEE Signal Processing Magazine*, vol. 39, no. 1, pp. 118–125, 2022.
- [16] J. Zhu, X. Lin, R.S. Blum, Y. Gu, "Parameter estimation from quantized observations in multiplicative noise environments," *IEEE Trans. Signal Processing*, vol. 63, no. 15, pp. 4037–4050, 2015.
- [17] F. Wang, J. Fang, H. Li, Z. Chen, and S. Li, "One-bit quantization design and channel estimation for massive MIMO systems," *IEEE Trans. Veh. Technol.*, vol. 67, no. 11, pp. 10 921–10 934, 2018.
- [18] H. C. Papadopoulos, G. W. Wornell, and A. V. Oppenheim, "Sequential signal encoding from noisy measurements using quantizers with dynamic bias control," *IEEE Trans. on Inf. Theory*, vol. 47, no. 3, pp. 978–1002, 2001.
- [19] L. Ni, D. Zhang, Y. Sun, N. Liu, J. Liang, and Q. Wan, "Detection and localization of one-bit signal in multiple distributed subarray systems," *IEEE Trans. Signal Processing*, vol. 71, pp. 2776–2791, 2023.
- [20] N. Harel and T. Routtenberg, "Non-Bayesian estimation with partially quantized observations," in *DSP*, 2017, pp. 1–5.
- [21] S. Sedighi, B. S. Mysore R, M. Soltanalian, and B. Ottersten, "On the performance of one-bit DoA estimation via sparse linear arrays," *IEEE Trans. Signal Processing*, vol. 69, pp. 6165–6182, 2021.
- [22] G. Zeitler, G. Kramer, and A. C. Singer, "Bayesian parameter estimation using single-bit dithered quantization," *IEEE Trans. Signal Processing*, vol. 60, no. 6, pp. 2713–2726, 2012.
- [23] S. Zeitz, F. Gast, M. Dorpinghaus, and G. Fettweis, "On the Bayesian Cramér–Rao bound for phase noise estimation based on 1-bit quantized samples," *IEEE Signal Process. Lett.*, Jan, 2023.
- [24] S. S. Thoota and C. R. Murthy, "Massive MIMO-OFDM systems with low resolution ADCs: Cramér–Rao bound, sparse channel estimation, and soft symbol decoding," *IEEE Trans. Signal Processing*, vol. 70, pp. 4835–4850, 2022.
- [25] Z. Shao, L. T. N. Landau, and R. C. Lamare, "Channel estimation using 1-bit quantization and oversampling for large-scale multiple-antenna systems," in *ICASSP*, 2019, pp. 4669–4673.
- [26] M. Stein, S. Bar, J. Nossek, and J. Tabrikian, "Performance analysis for channel estimation with 1-bit ADC and unknown quantization threshold," vol. 66, no. 10, pp. 2557–2571, 2018.
- [27] F. Liu, H. Zhu, C. Li, J. Li, P. Wang, and P. V. Orlik, "Angular-domain channel estimation for one-bit massive MIMO systems: Performance bounds and algorithms," *IEEE Trans. Veh. Technol.*, vol. 69, no. 3, pp. 2928–2942, 2020.
- [28] G. O. Balkan and S. Gezici, "CRLB based optimal noise enhanced parameter estimation using quantized observations," *IEEE Signal Process. Letters*, vol. 17, no. 5, pp. 477–480, 2010.
- [29] A. Vempaty, H. He, B. Chen, and P. K. Varshney, "On quantizer design for distributed Bayesian estimation in sensor networks," *IEEE Trans. Signal Processing*, vol. 62, no. 20, pp. 5359–5369, 2014.
- [30] S. Kar, H. Chen, and P. K. Varshney, "Optimal identical binary quantizer design for distributed estimation," *IEEE Trans. Signal Processing*, vol. 60, no. 7, pp. 3896–3901, 2012.
- [31] Y. Mazor, I. E. Berman, and T. Routtenberg, "On the limitations of the Bayesian Cramér–Rao bound for mixed-resolution data," *IEEE Signal Processing Letters*, vol. 32, pp. 446–450, 2025.
- [32] O. Aharon and J. Tabrikian, "Asymptotically tight Bayesian Cramér–Rao bound," *IEEE Trans. Signal Processing*, vol. 72, pp. 3333–3346, 2024.
- [33] I. E. Berman and T. Routtenberg, "Resource allocation and dithering of Bayesian parameter estimation using mixed-resolution data," *IEEE Trans. Signal Processing*, vol. 69, pp. 6148–6164, 2021.
- [34] P. J. Schreier and L. L. Scharf, *Statistical Signal Processing of Complex-Valued Data - the Theory of Improper and Noncircular Signals*. Cambridge University Press, 2010.
- [35] M. H. DeGroot and M. J. Schervish, *Probability and Statistics*. Addison-Wesley, 2010.
- [36] W. Rudin, *Real and Complex Analysis*. McGraw-Hill Book Company, 1966.
- [37] Q. Wan, J. Fang, H. Duan, Z. Chen, and H. Li, "Generalized Bussgang LMMSE channel estimation for one-bit massive MIMO systems," *IEEE Trans. Wireless Communications*, vol. 19, no. 6, pp. 4234–4246, 2020.
- [38] H. V. Habi, H. Messer, and Y. Bresler, "Learned Bayesian Cramér–Rao bound for unknown measurement models using score neural networks," *arXiv preprint arXiv:2502.00724*, 2025.
- [39] Z. Shao, L.T.N. Landau, R.C. LAMARE, "Channel estimation for large-scale multiple-antenna systems using 1-bit ADCs and oversampling," *IEEE Access*, vol. 8, pp. 85 243–85 256, 2020.
- [40] Diana M. V. Melo; Lukas T. N. Landau; Rodrigo C. de Lamare; Peter F. Neuhaus; Gerhard P. Fettweis, "Zero-crossing precoding techniques for channels with 1-bit temporal oversampling ADCs," *IEEE Tran. Wireless Communications*, vol. 22, pp. 5321–5336, 2023.
- [41] Y. Hu, J. Garcia-Frias, and M. Lamarca, "Analog joint source-channel coding using non-linear curves and MMSE decoding," *IEEE Trans. Communications*, vol. 59, no. 11, pp. 3016–3026, 2011.
- [42] A. Doucet, X. Wang, "Monte Carlo methods for signal processing: a review in the statistical signal processing context," *IEEE Signal Processing Magazine*, vol. 22, pp. 152–170, 2000.
- [43] C.P. Robert, G. Casella, "Monte Carlo Statistical Methods". Springer-Verlag, 2000.
- [44] Y. Hu, J. Garcia-Frias and M. Lamarca, "Analog joint source-channel coding using non-linear curves and MMSE decoding," *IEEE Trans. on Communications*, vol. 59, no. 11, pp. 3016–3026, 2011.
- [45] B. Fesl, M. Koller, and W. Utschick, "On the mean square error optimal estimator in one-bit quantized systems," *IEEE Trans. Signal Processing*, vol. 71, pp. 1968–1980, 2023.
- [46] M. Ding, I. Atzeni, A. Tölli and A.L. Swindlehurst, "On the optimal MMSE channel estimation for one-bit quantized MIMO systems," *IEEE Trans. Signal Processing*, vol. 73, pp. 617–632, 2025.
- [47] N. Shlezinger and T. Routtenberg, "Discriminative and generative learning for the linear estimation of random signals [lecture notes]," *IEEE Signal Processing Magazine*, vol. 40, no. 6, pp. 75–82, 2023.
- [48] J. Serra and M. Nájar, "Asymptotically optimal linear shrinkage of sample LMMSE and MVDR filters," *IEEE Trans. Signal Process.*, vol. 62, no. 14, p. 3552–3564, 2014.
- [49] Harry L. Van Trees, "Optimum array processing: Part IV of detection, estimation, and modulation theory". John Wiley and Sons, 2004.
- [50] M. Z. Ben Zion Bobrovsky, Eddy Mayer-Wolf, "Some classes of global Cramér–Rao bounds," *The Annals of Statistics*, 1987.
- [51] H. L. Van Trees and K. L. Bell, "Bayesian Bounds for Parameter Estimation and Nonlinear Filtering/Tracking". Wiley-IEEE Press, 2007.
- [52] S. Kay, "Fundamentals of Statistical Signal Processing: Estimation Theory". Prentice Hall, 1993.
- [53] A. Mezghani and J. A. Nossek, "On ultra-wideband MIMO systems with 1-bit quantized outputs: Performance analysis and input optimization," in *IEEE ISIT*, 2007, pp. 1286–1289.
- [54] Y. Bar-Shalom and A. Weiss, "DOA estimation using 1-bit quantized measurements," *IEEE Trans. Aerospace and Electronic Systems*, vol. 38, no. 3, pp. 868–884, 2002.
- [55] Y. Li, C. Tao, G. S.-G. A. Mezghani, A. L. Swindlehurst, and L. Liu, "Channel estimation and performance analysis of one-bit massive MIMO systems."
- [56] H. L. Van Trees, *Detection, Estimation, and Modulation Theory, Part I*. John Wiley & Sons, 2004.
- [57] F. Athley, "Threshold region performance of maximum likelihood doa estimation for a single source," in *Conference Record of the Thirty-Sixth Asilomar Conference on Signals, Systems and Computers*, 2002.
- [58] J. Park, S. Park, A. Yazdan, and R. W. Heath, "Optimization of mixed-ADC multi-antenna systems for cloud-RAN deployments," *IEEE Trans. on Communications*, vol. 65, no. 9, pp. 3962–3975, 2017.
- [59] I. E. Berman and T. Routtenberg, "Partially linear Bayesian estimation using mixed-resolution data," *IEEE Signal Process. Letters*, vol. 28, pp. 2202–2206, 2021.
- [60] L. Lu, G.Y. Li, A.L. Swindlehurst, A. Ashikhmin, R. Zhang, "An overview of massive MIMO: Benefits and challenges," *IEEE J. Sel. Top. Signal Process.*, vol. 8, no. 5, pp. 742–758, 2014.
- [61] A. HJØRUNGNES, *Complex-Valued Matrix Derivatives*. Cambridge University Press, 2011.
- [62] E. Ollila, V. Koivunen, and J. Eriksson, "On the Cramér–Rao bound for the constrained and unconstrained complex parameters," in *5th IEEE Sensor Array and Multichannel Signal Processing Workshop*, 2008.

Supplemental Material for “Weighted Bayesian Cramér–Rao Bound for Mixed-Resolution Parameter Estimation”

This document contains supplemental material for the paper. In the following, we present an extension of the proposed WBCRB in (55), and show that under the LGO model, it is sufficient to use only the standard WBCRB.

APPENDIX B

EXTENSION OF THE WBCRB ON THE AUGMENTED MSE

In the estimation of complex-valued parameters, the conventional MSE matrix is insufficient to fully characterize second-order statistics [62]. Instead, both the covariance and pseudo-covariance matrices should be considered. To this end, we define the augmented form as

$$\bar{\epsilon} = \left[(\hat{\theta}(\mathbf{x}_a, \mathbf{x}_q) - \theta)^T, (\hat{\theta}(\mathbf{x}_a, \mathbf{x}_q) - \theta)^H \right]^T.$$

The augmented MSE matrix is defined as

$$\mathbf{MSE}_{\text{aug}} = \mathbb{E} \left[(\bar{\epsilon} - \mathbb{E}[\bar{\epsilon}])(\bar{\epsilon} - \mathbb{E}[\bar{\epsilon}])^H \right] \in \mathbb{C}^{2M \times 2M}. \quad (80)$$

It can be seen that the upper-left $M \times M$ block of $\mathbf{MSE}_{\text{aug}}$ is the MSE matrix, $\mathbb{E} \left[(\hat{\theta}(\mathbf{x}_a, \mathbf{x}_q) - \theta)(\hat{\theta}(\mathbf{x}_a, \mathbf{x}_q) - \theta)^H \right]$, which is bounded in Theorem 1. The lower-right $M \times M$ block is the complex-conjugate of the MSE matrix. The off-diagonal $M \times M$ blocks are the pseudo-covariance of the estimation error vector, given by $\mathbb{E} \left[(\hat{\theta}(\mathbf{x}_a, \mathbf{x}_q) - \theta)(\hat{\theta}(\mathbf{x}_a, \mathbf{x}_q) - \theta)^T \right]$, and its complex conjugate. It should be noted that even if the true parameter vector θ is circularly symmetric (i.e., proper), the estimation error may still be an improper complex random vector, since the estimator is not constrained to be proper. In such cases, the conventional covariance matrix does not fully capture the second-order statistics, and it is necessary to consider the augmented error and provide a lower bound on the full augmented MSE matrix.

We now present the WBCRB on the augmented MSE (80) in a similar manner to Theorem 1, but using the augmented BFIM. In this case, we use the Hermitian, positive-definite weight matrix $\bar{\mathbf{W}}(\theta) \in \mathbb{C}^{2M \times 2M}$. Similar to (21), we define the vector $\bar{\mathbf{v}}(\theta) \in \mathbb{C}^{2M}$ with components

$$[\bar{\mathbf{v}}(\theta)]_k = \sum_{m=1}^{2M} \frac{\partial [\bar{\mathbf{W}}(\theta)]_{k,m}}{\partial \bar{\theta}_m^*},$$

where $\bar{\theta} = (\theta_1, \dots, \theta_M, \theta_1^*, \dots, \theta_M^*)^T$, and $\bar{\mathbf{A}} \in \mathbb{C}^{2M \times 2M}$ collects all derivatives of $\bar{\mathbf{W}}(\theta)$ as in (22):

$$[\bar{\mathbf{A}}]_{n,k} \triangleq -\mathbb{E} \left[\sum_{m=1}^{2M} \frac{\partial ([\bar{\mathbf{W}}(\theta)]_{n,m} \bar{v}_k^*(\theta))}{\partial \bar{\theta}_m^*} \right]. \quad (81)$$

In addition, define the augmented BFIM as [62]

$$\bar{\mathbf{J}} = \begin{bmatrix} \mathbf{J} & \mathbf{P} \\ \mathbf{P}^* & \mathbf{J}^* \end{bmatrix} \in \mathbb{C}^{2M \times 2M}, \quad (82)$$

where \mathbf{J} is the BFIM as given in (20), and the pseudo-information matrix is defined as (cf. [62])

$$\mathbf{P} \triangleq \mathbb{E} \left[\nabla_{\theta}^T \log p(\theta) p(\mathbf{x}_a | \theta) p(\mathbf{x}_q | \theta) \right] \times \nabla_{\theta} \log p(\theta) p(\mathbf{x}_a | \theta) p(\mathbf{x}_q | \theta). \quad (83)$$

This matrix can be decomposed into the prior, analog, and quantized contributions in a similar manner to the BFIM in (20). Finally, we define

$$\bar{\mathbf{G}} = \mathbb{E}[\bar{\mathbf{W}}(\theta) \bar{\mathbf{J}} \bar{\mathbf{W}}(\theta)] + \bar{\mathbf{A}} + \bar{\mathbf{A}}^H + \mathbb{E}[\bar{\mathbf{v}}(\theta) \bar{\mathbf{v}}^H(\theta)]. \quad (84)$$

Theorem 2 (Augmented WBCRB): Under the mixed-resolution model of Subsection II and Conditions 1–4, for any estimator $\hat{\theta}(\mathbf{x}_a, \mathbf{x}_q)$

$$\mathbf{MSE}_{\text{aug}} \succeq \mathbb{E}[\bar{\mathbf{W}}(\theta)] \bar{\mathbf{G}}^{-1} \mathbb{E}[\bar{\mathbf{W}}(\theta)]^H, \quad (85)$$

where $\bar{\mathbf{G}}$ is defined in (84).

Proof: The proof is similar to the proof in Appendix 1, with the following augmented auxiliary function:

$$\bar{\mathbf{g}}(\mathbf{x}_a, \mathbf{x}_q, \theta) = \bar{\mathbf{W}}(\theta) [\nabla_{\text{aug}} \log p]^H + \bar{\mathbf{v}}(\theta), \quad (86)$$

where the augmented score is defined as

$$\nabla_{\text{aug}} \log p = \begin{bmatrix} \nabla_{\theta} \log p(\theta, \mathbf{x}_a, \mathbf{x}_q) \\ \nabla_{\theta^*} \log p(\theta, \mathbf{x}_a, \mathbf{x}_q) \end{bmatrix} \in \mathbb{C}^{2M}. \quad (87)$$

The upper-left $M \times M$ block of the bound on the r.h.s. of (85) provides a lower bound on the ordinary MSE, while the off-diagonal blocks bound the pseudo-covariance of the error. If the pseudo-information in $\bar{\mathbf{J}}$ (defined in (83)) vanishes, the augmented bound decouples into two identical real-valued WBCRBs on the covariance of the real and imaginary parts. In this case, the upper-left $M \times M$ block of the bound coincides with the WBCRB from Theorem 1.

As an example, it can be seen that the inverse of $\bar{\mathbf{J}}$ is given by (see Equation (8) in [62])

$$\bar{\mathbf{J}}^{-1} = \begin{bmatrix} \mathcal{R}^{-1} & -\mathcal{R}^{-1} \mathcal{Q} \\ -\mathcal{Q}^H \mathcal{R}^{-1} & \mathcal{R}^{-1*} \end{bmatrix}, \quad (88)$$

where \mathcal{R} is the associated Schur complement, defined as $\mathbf{J} - \mathbf{P}(\mathbf{J}^{-1})^* \mathbf{P}^*$, and $\mathcal{Q} \triangleq \mathbf{P}(\mathbf{J}^{-1})^*$. This formulation coincides with the widely linear BCRB, which is generally tighter than the ordinary BCRB [34, p. 168].

APPENDIX C

EXTENSION OF THE WBCRB ON THE AUGMENTED MSE UNDER THE LGO MODEL

Theorem 3: Under the LGO model and under the conditions from Section IV-A, the pseudo-information matrix \mathbf{P} (83) vanishes.

Proof: The conditional log-likelihood function for the considered model is given in (3). Using a similar derivation as for \mathbf{J} in [31], it can be shown that the pseudo-information matrix \mathbf{P} , defined in (83), satisfies

$$\mathbf{P} = \mathbf{P}_{\theta} + \mathbb{E}_{\theta}[\mathbf{P}_{\mathbf{x}_a | \theta}] + \mathbb{E}_{\theta}[\mathbf{P}_{\mathbf{x}_q | \theta}]. \quad (89)$$

The pseudo-information matrices based on each set of measurements \mathbf{x}_a and \mathbf{x}_q given θ are defined as:

$$\mathbf{P}_{\mathbf{x}_a | \theta} \triangleq \mathbb{E}_{\mathbf{x}_a | \theta} \left[\nabla_{\theta}^T \log p(\mathbf{x}_a | \theta) \nabla_{\theta} \log p(\mathbf{x}_a | \theta) \right], \quad (90a)$$

$$\mathbf{P}_{\mathbf{x}_q | \theta} \triangleq \mathbb{E}_{\mathbf{x}_q | \theta} \left[\nabla_{\theta}^T \log p(\mathbf{x}_q | \theta) \nabla_{\theta} \log p(\mathbf{x}_q | \theta) \right]. \quad (90b)$$

Furthermore, θ is a circularly symmetric Gaussian vector, and $\mathbf{x}_a | \theta \sim \mathcal{CN}(\mathbf{H}\theta, \sigma_a^2 \mathbf{I}_{N_a})$. Thus, it follows immediately that

$\mathbf{P}_{\mathbf{x}_q|\boldsymbol{\theta}}$ and $\mathbf{P}_{\boldsymbol{\theta}} = \mathbf{0}$ vanish (note that the conditional distribution $p(\mathbf{x}_q|\boldsymbol{\theta})$ is a complex, circularly symmetric Gaussian). By substituting these results in (89), we obtain that for the considered model $\mathbf{P} = \mathbb{E}_{\boldsymbol{\theta}}[\mathbf{P}_{\mathbf{x}_q|\boldsymbol{\theta}}]$.

To complete the proof, it remains to show that $\mathbb{E}_{\boldsymbol{\theta}}[\mathbf{P}_{\mathbf{x}_q|\boldsymbol{\theta}}]$ in (90b) vanishes as well.

The 1-bit quantized log-likelihood function is equal to

$$\begin{aligned} \log p(\mathbf{x}_q|\boldsymbol{\theta}) = & \sum_{n=1}^{N_q} \left(\frac{1}{2} + \frac{\text{Re}\{\mathbf{x}_{q_n}\}}{\sqrt{2}} \right) \log \Phi(\zeta_n^R) \\ & + \left(\frac{1}{2} - \frac{\text{Re}\{\mathbf{x}_{q_n}\}}{\sqrt{2}} \right) \log(1 - \Phi(\zeta_n^R)) \\ & + \left(\frac{1}{2} + \frac{\text{Im}\{\mathbf{x}_{q_n}\}}{\sqrt{2}} \right) \log \Phi(\zeta_n^I) \\ & + \left(\frac{1}{2} - \frac{\text{Im}\{\mathbf{x}_{q_n}\}}{\sqrt{2}} \right) \log(1 - \Phi(\zeta_n^I)), \quad (91) \end{aligned}$$

and it can be verified that the complex-valued gradient of the quantized measurements' log-likelihood from (91) is

$$\begin{aligned} \nabla_{\boldsymbol{\theta}}^T \log p(\mathbf{x}_q|\boldsymbol{\theta}) = & \frac{1}{\sqrt{2}\sigma_q} \sum_{n=1}^{N_q} \mathbf{g}_n \\ & \times \left[\frac{\phi(\zeta_n^R)}{\Phi(\zeta_n^R)(\Phi(\zeta_n^R) - 1)} \left(\Phi(\zeta_n^R) - \frac{1}{2} - \frac{1}{\sqrt{2}} \text{Re}\{\mathbf{x}_{q_n}\} \right) \right. \\ & \left. - j \frac{\phi(\zeta_n^I)}{\Phi(\zeta_n^I)(\Phi(\zeta_n^I) - 1)} \left(\Phi(\zeta_n^I) - \frac{1}{2} - \frac{1}{\sqrt{2}} \text{Im}\{\mathbf{x}_{q_n}\} \right) \right], \quad (92) \end{aligned}$$

where ζ_n^R and ζ_n^I are defined in (54). Furthermore, the mean of the real and imaginary parts of \mathbf{x}_{q_n} given $\boldsymbol{\theta}$ is given by

$$\sqrt{2}\mathbb{E}[\text{Re}\{\mathbf{x}_{q_n}\}|\boldsymbol{\theta}] = 2\Phi(\zeta_n^R) - 1, \quad (93a)$$

$$\sqrt{2}\mathbb{E}[\text{Im}\{\mathbf{x}_{q_n}\}|\boldsymbol{\theta}] = 2\Phi(\zeta_n^I) - 1, \quad (93b)$$

respectively. The second moment for both parts is equal to

$$\mathbb{E}[\text{Re}^2\{\mathbf{x}_{q_n}\}|\boldsymbol{\theta}] = \mathbb{E}[\text{Im}^2\{\mathbf{x}_{q_n}\}|\boldsymbol{\theta}] = 0.5. \quad (94)$$

We note that the smoothness assumption is valid for quantized measurements since the expected value of the gradient is zero, as shown using (93a), (93b), and (94).

Substituting (92) into $\mathbf{P}_{\mathbf{x}_q|\boldsymbol{\theta}}$ and utilizing (93) and (94), along with the fact that the entries of $\mathbf{x}_q|\boldsymbol{\theta}$ are independent and their real and imaginary parts are also independent, we

obtain that

$$\begin{aligned} \mathbf{P}_{\mathbf{x}_q|\boldsymbol{\theta}} = & \frac{1}{2\sigma_q^2} \sum_{n=1}^{N_q} \mathbb{E}_{\mathbf{x}_q|\boldsymbol{\theta}} \left[\left(\frac{\phi(\zeta_n^R) \left(\Phi(\zeta_n^R) - \frac{1}{2} - \frac{1}{\sqrt{2}} \text{Re}\{\mathbf{x}_{q_n}\} \right)}{\Phi(\zeta_n^R)(\Phi(\zeta_n^R) - 1)} \right)^2 \right. \\ & - 2j \left(\frac{\phi(\zeta_n^R) \left(\Phi(\zeta_n^R) - \frac{1}{2} - \frac{1}{\sqrt{2}} \text{Re}\{\mathbf{x}_{q_n}\} \right)}{\Phi(\zeta_n^R)(\Phi(\zeta_n^R) - 1)} \right) \\ & \left. \left(\frac{\phi(\zeta_n^I) \left(\Phi(\zeta_n^I) - \frac{1}{2} - \frac{1}{\sqrt{2}} \text{Im}\{\mathbf{x}_{q_n}\} \right)}{\Phi(\zeta_n^I)(\Phi(\zeta_n^I) - 1)} \right) \right. \\ & \left. - \left(\frac{\phi(\zeta_n^I) \left(\Phi(\zeta_n^I) - \frac{1}{2} - \frac{1}{\sqrt{2}} \text{Im}\{\mathbf{x}_{q_n}\} \right)}{\Phi(\zeta_n^I)(\Phi(\zeta_n^I) - 1)} \right)^2 \right] \mathbf{g}_n \mathbf{g}_n^T \\ = & \frac{1}{2\sigma_q^2} \sum_{n=1}^{N_q} \left[\mathbb{E}_{\mathbf{x}_q|\boldsymbol{\theta}} \left[\left(\frac{\phi(\zeta_n^R) \left(\Phi(\zeta_n^R) - \frac{1}{2} - \frac{1}{\sqrt{2}} \text{Re}\{\mathbf{x}_{q_n}\} \right)}{\Phi(\zeta_n^R)(\Phi(\zeta_n^R) - 1)} \right)^2 \right. \right. \right. \\ & \left. \left. - \left(\frac{\phi(\zeta_n^I) \left(\Phi(\zeta_n^I) - \frac{1}{2} - \frac{1}{\sqrt{2}} \text{Im}\{\mathbf{x}_{q_n}\} \right)}{\Phi(\zeta_n^I)(\Phi(\zeta_n^I) - 1)} \right)^2 \right] \right. \\ & \left. - 2j \mathbb{E}_{\mathbf{x}_q|\boldsymbol{\theta}} \left[\left(\frac{\phi(\zeta_n^R) \left(\Phi(\zeta_n^R) - \frac{1}{2} - \frac{1}{\sqrt{2}} \text{Re}\{\mathbf{x}_{q_n}\} \right)}{\Phi(\zeta_n^R)(\Phi(\zeta_n^R) - 1)} \right) \right. \right. \right. \\ & \left. \left. \mathbb{E}_{\mathbf{x}_q|\boldsymbol{\theta}} \left[\left(\frac{\phi(\zeta_n^I) \left(\Phi(\zeta_n^I) - \frac{1}{2} - \frac{1}{\sqrt{2}} \text{Im}\{\mathbf{x}_{q_n}\} \right)}{\Phi(\zeta_n^I)(\Phi(\zeta_n^I) - 1)} \right) \right] \right] \mathbf{g}_n \mathbf{g}_n^T \right. \\ & \left. = \frac{1}{2\sigma_q^2} \sum_{n=1}^{N_q} \left(\frac{\phi^2(\zeta_n^R)}{\Phi(\zeta_n^R)\Phi(-\zeta_n^R)} - \frac{\phi^2(\zeta_n^I)}{\Phi(\zeta_n^I)\Phi(-\zeta_n^I)} \right) \mathbf{g}_n \mathbf{g}_n^T, \quad (95) \right. \end{aligned}$$

where we used the fact that

$$\mathbb{E}[\text{Re}\{\mathbf{x}_{q_n}\}\text{Im}\{\mathbf{x}_{q_n}\}|\boldsymbol{\theta}] = \mathbb{E}[\text{Re}\{\mathbf{x}_{q_n}\}|\boldsymbol{\theta}]\mathbb{E}[\text{Im}\{\mathbf{x}_{q_n}\}|\boldsymbol{\theta}].$$

Thus, we have

$$\begin{aligned} \mathbb{E}_{\boldsymbol{\theta}}[\mathbf{P}_{\mathbf{x}_q|\boldsymbol{\theta}}] = & \frac{1}{2\sigma_q^2} \sum_{n=1}^{N_q} \left(\mathbb{E}_{\boldsymbol{\theta}} \left[\frac{\phi^2(\zeta_n^R)}{\Phi(\zeta_n^R)\Phi(-\zeta_n^R)} \right] - \right. \\ & \left. \mathbb{E}_{\boldsymbol{\theta}} \left[\frac{\phi^2(\zeta_n^I)}{\Phi(\zeta_n^I)\Phi(-\zeta_n^I)} \right] \right) \mathbf{g}_n \mathbf{g}_n^T = \mathbf{0}. \quad (96) \end{aligned}$$

Assuming, in addition, that the off-diagonal blocks of the matrix $\mathbf{A} + \mathbf{A}^H + \mathbb{E}[\mathbf{v}(\boldsymbol{\theta})\mathbf{v}^H(\boldsymbol{\theta})]$ are zero, which is a condition that can be ensured by selecting an appropriate weight matrix, this claim justifies focusing solely on the l.h.s. of (24), as is widely considered in the relevant literature. In the context of the conventional BCRB (27), this result further implies that the widely linear BCRB from [34, eq. 6.64], which generally offers a tighter bound than the standard BCRB, reduces to the traditional form and becomes equal to the BCRB, as formalized in Corollary 1 of [62].